

## Magneto-hydrodynamically stable axisymmetric mirrors<sup>a)</sup>

D. D. Ryutov,<sup>1,b)</sup> H. L. Berk,<sup>2</sup> B. I. Cohen,<sup>1</sup> A. W. Molvik,<sup>1</sup> and T. C. Simonen<sup>3</sup>

<sup>1</sup>Lawrence Livermore National Laboratory, Livermore, California 94551, USA

<sup>2</sup>University of Texas, Austin, Texas 78712, USA

<sup>3</sup>University of California, Berkeley, California 94720, USA

(Received 23 April 2011; accepted 20 July 2011; published online 1 September 2011)

Making axisymmetric mirrors magnetohydrodynamically (MHD) stable opens up exciting opportunities for using mirror devices as neutron sources, fusion-fission hybrids, and pure-fusion reactors. This is also of interest from a general physics standpoint (as it seemingly contradicts well-established criteria of curvature-driven instabilities). The axial symmetry allows for much simpler and more reliable designs of mirror-based fusion facilities than the well-known quadrupole mirror configurations. In this tutorial, after a summary of classical results, several techniques for achieving MHD stabilization of the axisymmetric mirrors are considered, in particular: (1) employing the favorable field-line curvature in the end tanks; (2) using the line-tying effect; (3) controlling the radial potential distribution; (4) imposing a divertor configuration on the solenoidal magnetic field; and (5) affecting the plasma dynamics by the ponderomotive force. Some illuminative theoretical approaches for understanding axisymmetric mirror stability are described. The applicability of the various stabilization techniques to axisymmetric mirrors as neutron sources, hybrids, and pure-fusion reactors are discussed; and the constraints on the plasma parameters are formulated. © 2011 American Institute of Physics. [doi:10.1063/1.3624763]

### I. INTRODUCTION

Mirror confinement devices also called sometimes “open-ended devices” to distinguish them from toroidal (“closed”) devices have been studied since the early days of fusion research. The concept of a mirror device is based on a linear geometry, with two (or more) zones of increased magnetic field near the ends (Fig. 1), which reflect a significant fraction of plasma particles escaping the device along the axis (whence “mirrors”). Reviews of mirror research until the early 1990s, with extensive bibliography, can be found in Refs. 1–4.

The operation of mirror devices is, in principle, very simple: particles and energy are injected into a long solenoidal section of the device, which produce some fusion output (which depends, of course, on the quality of the confinement) and are eventually lost through the ends. There is no need of driving an external electric current in the plasma, the magnetic field is steady-state, and the heat loads at the end-walls can be made as low as desired by using a strong flaring of the magnetic flux in the end tanks.

In order to make the plasma magneto-hydrodynamically (MHD) stable, an approach based on a “minimum B” geometry was used for decades. This approach (pioneered by the Ioffe group<sup>5</sup>) has led to development of a quadrupole magnetic geometry and spectacular success of the 2XIIB experiment at Livermore,<sup>6–8</sup> where a plasma with the ion temperature of 10 keV and the parameter  $\beta$  (the ratio of the plasma pressure to the magnetic pressure) approaching 1 was obtained. In the tandem mirror devices,<sup>9,10</sup> the stability was

provided by a set of complex coils of quadrupole symmetry similar to those shown in Fig. 2.

This stabilization technique, although certainly effective, was not without drawbacks. The structure of the field coils needed for creating this geometry was quite complex, as seen from Fig. 2. The use of such coils has led to significant limitations on the achievable magnetic field strength in the confinement zone: the currents required for creating the desired field strength were high, as were the complex mechanical stresses, thereby limiting the capabilities of coils, especially superconducting coils. The particle orbits were complex and could cause enhanced neoclassical and resonant transport.<sup>11</sup> A strong fanning of the magnetic field in transition zones led to decrease of the plasma thickness in these fanning zones, reducing the pressure limit for the onset of the ballooning instability<sup>12,13</sup> and also making the plasma more permeable to neutral gas. Although these difficulties were not lethal, they certainly did not help the mirror approach to fusion.

The desirability of making purely axisymmetric mirrors was clear, and some promising ideas have been put forward (see below) but the virtual termination of the US mirror program in 1986 did not allow for consistent experimental testing of these ideas and/or their more detailed theory analysis.

The work on axisymmetric mirrors continued in Russia, at the Budker Institute at Novosibirsk. A medium-scale axisymmetric mirror device called the gas-dynamic trap (GDT) (Ref. 14) was built there, with the stability provided by an outflowing plasma and other techniques (see below). At present, this device routinely operates at a plasma beta exceeding 0.5, ion temperature of  $\sim 10$  keV, and electron temperature  $T_e$  above 200 eV.<sup>15</sup> This facility can serve as a prototype for a neutron source for neutronic tests and qualifications of

<sup>a)</sup>Paper CT3 1, Bull. Am. Phys. Soc. 55, 61 (2010).

<sup>b)</sup>Invited Speaker.

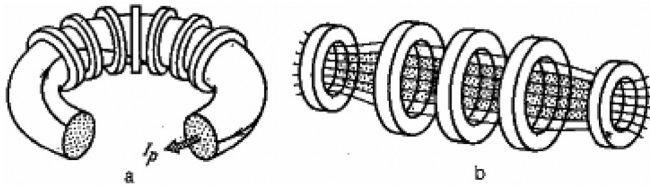


FIG. 1. Closed (a) and open (b) magnetic configurations. In the second case, the zones of a high magnetic field near the ends of the device are called “mirrors.” Sometimes, the word “mirror” is used to describe the whole device of this type.

materials and subcomponents of future fusion reactors.<sup>16</sup> Even without any significant extrapolation from the already achieved parameters, one can make a neutron source, which would produce a neutron flux of order of  $0.25 \text{ MW/m}^2$  (equivalent to  $2.2 \times 10^{13} \text{ n/cm}^2\text{s}$ ) over approximately  $1 \text{ m}^2$  test zone. With a modest extrapolation, it may be possible to develop a source producing  $2 \text{ MW/m}^2$  neutron flux, operating in a continuous mode and not requiring the tritium breeding (e.g., Ref. 17 and references therein). Another important mission that can be accomplished with the GDT (or analogous facility) is its use as an experimental platform for testing other stabilization techniques, which would be more suitable for future fusion reactors based on mirrors.

Development of an axisymmetric mirror system scalable to a fusion reactor would be a game-changer in fusion research.<sup>18</sup> Specifically, this device would possess the following properties: (1) It would be very attractive from the engineering standpoint, allowing for more space for shielding and simpler blanket geometries. (2) It would allow for high mirror ratios, thereby improving axial confinement and leading to a more flexible design. In particular, the higher

mirror ratio leads to a significant reduction of the size of a loss-cone “hole” in the velocity space, thereby improving the plasma stability with respect to the modes driven by the deviations of the distribution function from the isotropy. (3) The axisymmetry of the field would eliminate neoclassical and resonant transport. (4) Due to the engineering simplicity, the development process would accelerate: the turn-around time for testing various improvements would become much shorter than for more complex fusion systems.

Added to those are the already mentioned general advantages of mirrors (inherently steady state, no driven currents and associated disruptions, no problem with exhaust power handling).

One of the misconceptions associated with the mirror confinement is that the electron axial heat losses are too high and make it impossible for the mirror devices to reach fusion-relevant electron temperatures. It is sometimes stated that, as the plasma is in a contact with end-walls, the electrons will rapidly lose their energy. However, there is always an ambipolar potential in the end tanks, which guarantees a fulfillment of the quasineutrality constraint: only one electron is lost per a singly charged ion. This potential barrier is a few electron temperatures high. Then, each electron takes away from the trap an energy roughly equal to  $(5-6)T_e$ . In other words, when an ion is lost through the end, the energy loss is equal to the lost ion energy (typically,  $1-2T_i$ ), plus  $(5-6)T_e$  carried away by the accompanying electron. The loss at this rate had always been folded into the energy balance equations in the studies of mirror confinement and gave rise to a favorable energy balance. A review of the collisional losses from mirrors can be found in Ref. 19.

Of course, in order for the quasineutrality constraint to work in this fashion, one needs to have a good-enough vacuum in the end tank, so that the neutral gas density in the tank would be sufficiently small: otherwise, the ionization of this gas would produce a number of cold electrons which would be able to substitute hot electrons lost from the confinement zone. The hot electrons will then be lost at a rate exceeding the ion loss rate from the trap, leading to the decrease of  $T_e$  at a given input power. A similar issue may arise if the secondary emission from the end-plates is too high. The latter problem can be resolved by using expansion tanks with a sufficiently large expansion ratio  $K$  defined as the ratio of the mirror magnetic field and the magnetic field at the end-plate. Then, the secondary electrons will be largely reflected back to the wall because of a high mirror ratio ( $K$ ) they would have to overcome to penetrate into the hotter plasma. More details on these problems and further references can be found in Refs. 20 and 21. The low electron temperature in some of the earlier mirror experiments was not a reflection of some intrinsic failure of mirrors, but rather a result of a particular operational mode. In the current experiments with the GDT facility, the electron temperature closely follows classical predictions and is indeed determined by the balance between the heating sources and losses over the ambipolar potential in the end tank.<sup>22</sup>

This paper provides a brief tutorial on the stability of axisymmetric mirrors. We concentrate on the stability of the low- $\beta$  plasma. There are two reasons for that. First, the

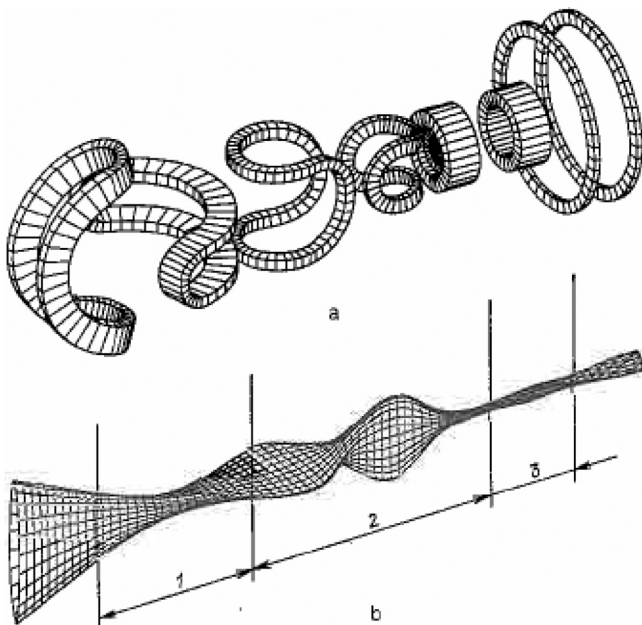


FIG. 2. The quadrupole mirror system of the MFTF-B facility: (a) the magnet system; (b) one of the flux surfaces. Zone 1 is the MHD-stable “anchor,” and zone 3 is an almost axisymmetric ambipolar “plug,” whereas zone 2 is a transition region; the central solenoid begins at the right upper corner and is terminated at the opposite end by the same complex system reversed left to right and rotated by  $90^\circ$  around the magnetic axis.

TABLE I. Characteristic parameters of mirror devices.<sup>a</sup>

	$L$ , m	$a_0$ , m	$B_0$ , T	$B_{mir}$ , T	$T_i$ ( $T_i^*$ ) (keV)	$T_e$ (keV)	$n_e$ , cm <sup>-3</sup>	$\tau_E$ , s	$\Gamma_0$ , s <sup>-1</sup>
GDT device <sup>b</sup>	7	0.08	0.3	<15	0.25 (7)	0.25	$5 \times 10^{13}$	0.003	$2 \times 10^5$
Neutron source <sup>b</sup>	12	0.15	2	15	1 (50)	1	$10^{14}$	0.03	$3 \times 10^5$
Hybrid driver	40	0.5	3	15	40	3	$10^{14}$	1	$10^5$
Pure fusion <sup>c</sup>	150	1.0	3	20	20	20	$5 \times 10^{13}$	20	$2 \times 10^4$

<sup>a</sup>Notation:  $L$  – mirror-to-mirror length,  $a_0$  – plasma radius in the midplane,  $B_0$  – the magnetic field in the midplane,  $B_{mir}$  – the magnetic field in the mirror throat,  $T_i$  – the ion temperature ( $T_i^*$  – the temperature of a hot ion component, if present),  $n_e$  – electron density in the midplane,  $\tau_E$  – energy confinement time,  $\Gamma_0$  – growth rate of the flute instability.

<sup>b</sup>Significant amount of a hot ion component is present.

<sup>c</sup>Central cell of a tandem mirror.

prevalent low- $\beta$  instability, the flute (or interchange) instability, if present, is so rapid that makes creation of a plasma with interesting parameters virtually impossible. The destructiveness of the flute instability has shown up in several early mirror experiments, including the one on a large-scale mirror facility OGRA.<sup>23</sup> Second, it turns out that, as soon as a robust stability with respect to the interchange mode is ensured, the pressure limit for the finite-beta modes in axisymmetric systems is typically high,  $\beta \sim 1$ , and does not impose any particularly stringent limits on the plasma operation. Still, for completeness, we provide a brief discussion of the finite-beta effects in Sec. VIII.

The structure of this tutorial is as follows: In Secs. II and III, which are key sections of this paper, the theory basis for the MHD equilibrium and stability of axisymmetric mirrors is described in a compact form. We feel that for a subject that was largely neglected for the last 20 or so years such an introduction is necessary. New consistent derivations of stability criteria and growth rates are presented, with explanations that are intended to provide some qualitative insights. Expressions for the parallel currents suitable for further use in subsequent sections are derived. A practically important case of a “long-thin” (paraxial) plasma is considered, and stability criteria and growth rates are presented in a closed form for small-scale perturbations. The simplest version of the stability criterion for a plasma with a sharp boundary is derived. In Sec. IV, the role of finite Larmor radius (FLR) effects is discussed. The exceptional role of the global mode is elucidated, and the quantitative analysis of the growth rate is presented. In Sec. V, stabilization of an axisymmetric mirror by the favorable curvature effects in the end tanks and in the confinement zone is discussed. Section VI is concerned with the stability control by the electric contact of the plasma with the end walls, including line-tying stabilization and controlled plasma rotation. Section VII describes non-paraxial stabilization via the use of short-fat mirrors or divertor stabilizers. Finite-beta effects and ballooning modes are considered in Sec. VIII. Other possible stabilization techniques are considered in Sec. IX. Section X contains discussion and a summary. The original results and new insights are present in Secs. III–IX.

This is a paper focused on stabilization concepts and theory models, not on a discussion of specific experiments. Still, we provide some key experimental references which could serve as a starting point for further searches.

Future mirror devices (neutron sources, drivers for fusion-fission hybrids, and pure-fusion reactors) cover a broad range of plasma parameters. The optimum stabilization techniques may differ from one system to another. In specific examples, we use the set of key parameters from Table I. The numbers presented in the table correspond to some generic versions of the facilities mentioned, not the numbers for specific designs or operational modes.

## II. AXISYMMETRIC EQUILIBRIA

As was mentioned in the Introduction, our main concern will be the low-beta plasma stability. However, for completeness, we mention also some problems of the finite-beta plasmas. In particular, in this section, axisymmetric equilibria of the plasma with finite beta are described. Later in the paper, in Sec. VIII, we consider both the possible use of the finite-beta effects to stabilize the plasma and the features of ballooning instabilities.

The general shape of an unperturbed system is shown in Figures 1(b) and 3. We use cylindrical coordinates  $r$ ,  $\vartheta$ ,  $z$ , with the axis  $z$  coinciding with the symmetry axis of an unperturbed system.

We introduce a unit vector  $\mathbf{t}$  collinear to the magnetic field  $\mathbf{B}$ ,  $\mathbf{t} = \mathbf{B}/B$ . The outer normal to the flux surface is denoted by  $\mathbf{n}$  (Fig. 3) A field-line curvature  $\kappa$  will be considered as positive for the concave field lines, so that

$$\kappa \mathbf{n} = (\mathbf{t} \cdot \nabla) \mathbf{t}. \quad (1)$$

The concave and convex regions of the field lines are indicated in Fig. 3(a). We introduce a binormal to the field line according to  $\mathbf{b} = \mathbf{t} \times \mathbf{n}$ , so that the unit vectors  $\mathbf{n}$ ,  $\mathbf{b}$ ,  $\mathbf{t}$  form a right triplet.

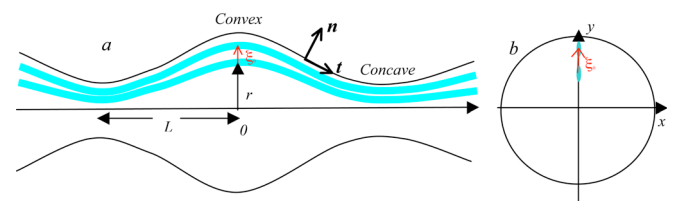


FIG. 3. (Color online) Cross-sections of the mirror device: (a) meridional cross-section; (b) equatorial cross section. A thick line represents a flux tube moved radially to a new location;  $\xi_0$  is the radial displacement in the equatorial plane. The maximum MHD growth rate corresponds to flux-tubes having ribbon-like shape (narrow in the azimuthal direction, panel b).

We denote by  $2\pi\Psi$ , the magnetic flux within a certain axisymmetric flux surface. Note the presence of the factor  $2\pi$ , which allows one to eliminate the same factor in a number of equations below. The position of a point on a certain flux surface can be characterized by an azimuthal angle  $\vartheta$  and a distance  $\ell$  measured along the field line from the mid-plane of the device.

As the plasma in the mirror devices is usually anisotropic, we consider a pressure in a tensorial form (see, e.g., Ref. 24):

$$p_{\alpha\beta} = p_{\perp}(\delta_{\alpha\beta} - t_{\alpha}t_{\beta}) + p_{\parallel}t_{\alpha}t_{\beta}. \quad (2)$$

This representation of the pressure tensor implies zero ion gyroradius. We later introduce additional terms, including the off-diagonal elements responsible for FLR stabilization. The components of the pressure tensor are related to the distribution functions of plasma particles

$$p_{\parallel} = \sum_{\nu} \int m_{\nu} v_{\parallel}^2 f_{\nu} d^3\mathbf{v}; \quad p_{\perp} = \sum_{\nu} \frac{1}{2} \int m_{\nu} v_{\perp}^2 f_{\nu} d^3\mathbf{v} \quad (3)$$

with summation carried out over the plasma species. The condition of the equilibrium along the field lines,  $t_{\alpha} \partial p_{\alpha\beta} / \partial x_{\beta} = 0$ , yields (Appendix A)

$$\frac{\partial p_{\parallel}}{\partial \ell} = \frac{p_{\parallel} - p_{\perp}}{B} \frac{\partial B}{\partial \ell}. \quad (4)$$

The projection of the equilibrium equation onto the normal  $\mathbf{n}$  reads as  $n_{\alpha} \partial / \partial x_{\beta} (p_{\alpha\beta} + T_{\alpha\beta}) = 0$ , where  $T_{\alpha\beta}$  is a Maxwell stress tensor,  $T_{\alpha\beta} = (B^2/8\pi)(\delta_{\alpha\beta} - 2t_{\alpha}t_{\beta})$  (e.g., Ref. 25). This equilibrium condition can be transformed to (Appendix A)

$$\frac{\partial}{\partial n} \left( p_{\perp} + \frac{B^2}{8\pi} \right) + \kappa \left( p_{\parallel} - p_{\perp} - \frac{B^2}{8\pi} \right) = 0, \quad (5)$$

where  $\partial/\partial n \equiv (\mathbf{n} \cdot \nabla)$  denotes the normal derivative, and  $\kappa$  is a field-line curvature defined according to Eq. (1). The projection of the equilibrium equation onto the bi-normal is satisfied in the axisymmetric case identically.

In the low-pressure case, when the parameter  $\beta \equiv 8\pi p/B^2$  is small, one can neglect the perturbation of the magnetic field by the plasma pressure and consider the field as curl-free  $\nabla \times \mathbf{B} = 0$ . As Eqs. (A1)–(A2) in Appendix A show, for the curl-free magnetic field,

$$\kappa = \frac{1}{B} \frac{\partial B}{\partial n}. \quad (6)$$

In the low-beta case, it is convenient to introduce, instead of a coordinate  $\ell$ , a closely related quantity  $s = \int B d\ell$ , with the integration performed along a field line from the equatorial plane to the observation point. One can check that for the vacuum (curl-free) magnetic field, the coordinate surfaces  $s = \text{const}$  are orthogonal to the surfaces  $\Psi = \text{const}$  (whereas a coordinate surface  $\ell = \text{const}$  is not necessarily orthogonal to the coordinate surface  $\Psi = \text{const}$ , this being somewhat inconvenient). The

quantity  $s$  is a scalar potential of the magnetic field. For any function  $f(\Psi, s)$  one has

$$\frac{\partial f(\Psi, s)}{\partial \Psi} = \frac{1}{Br} \frac{\partial f}{\partial n}. \quad (7)$$

Note that with our definition of  $\Psi$ , the factor of  $2\pi$  is absent from Eq. (7). Equation (6) can be written as

$$\kappa = -rB^2 \frac{\partial}{\partial \Psi} \left( \frac{1}{B(\Psi, s)} \right). \quad (8)$$

### III. GENERAL ISSUES OF AXISYMMETRIC STABILITY OF A LOW-PRESSURE PLASMA

As explained in Introduction, the critical issue that determines the very possibility of good performance of axisymmetric mirrors is that of the plasma stability at a low beta. This and several subsequent sections address this issue. The effects of the finite beta are described in Sec. VIII.

As is obvious from Eq. (6) and Fig. 3, for negative curvature,  $B$  decreases away from the plasma boundary and vice versa for positive curvature. As the transverse particle energy  $W_{\perp} = \mu B$ , with  $\mu$  being the adiabatic invariant (magnetic moment), decreases together with  $B$ , the particles confined near the midplane of a mirror machine release their energy when moving away from the axis, thereby providing a source of energy to drive an instability. For this reason, the positive curvature is called ‘‘favorable’’ and negative curvature ‘‘unfavorable.’’ This qualitative picture was presented in the groundbreaking paper by Rosenbluth and Longmire<sup>26</sup> and helps a lot in assessing the stability issues.

#### A. Equations for perturbations

The perturbation is characterized by the displacement vector  $\xi$ . We seek perturbations in the form  $\exp(-i\omega t + im\vartheta)f(r, z)$ , with  $\omega$  being a complex frequency and  $m$  being the azimuthal mode number. Note that in a low-beta plasma, the vector  $\mathbf{B}$  and, accordingly, the vector  $\mathbf{t}$  are not perturbed, so that  $\delta p_{\alpha\beta} = \delta p_{\perp}(\delta_{\alpha\beta} - t_{\alpha}t_{\beta}) + \delta p_{\parallel}t_{\alpha}t_{\beta}$ . The perturbed momentum equation reads as

$$-\omega^2 \rho \xi = \delta f + \delta f_{add} + \frac{\delta \mathbf{j} \times \mathbf{B}}{c}, \quad (9)$$

where  $\delta f$  is the perturbation of the pressure force stemming from the diagonal pressure tensor (2) and  $\delta f_{add}$  describes perturbations of other possible forces, in particular the ones stemming from the off-diagonal elements of the momentum flux tensor, as well as ponderomotive forces generated by external sources, like atomic beams, radio-frequency waves, etc. For now, we ignore the term  $\delta f_{add}$  and focus on the force  $\delta f$ . Note also that we neglect the magnetic field perturbation: the corresponding terms would be by a factor  $\beta$  smaller than the retained terms. Using standard equations of vector analysis (Appendix A), one can show that

$$\begin{aligned} \delta f = & -\nabla \delta p_{\perp} - \mathbf{t}(\mathbf{t} \cdot \nabla)(\delta p_{\parallel} - \delta p_{\perp}) \\ & - (\delta p_{\parallel} - \delta p_{\perp})[\mathbf{t} \nabla \cdot \mathbf{t} + (\mathbf{t} \cdot \nabla)\mathbf{t}]. \end{aligned} \quad (10)$$

Next we use the induction equation for the perfectly conducting plasma,  $\partial \mathbf{B} / \partial t = \nabla \times [\mathbf{v} \times \mathbf{B}]$ . Linearizing it, we find:  $\delta \mathbf{B} = \nabla \times [\boldsymbol{\xi} \times \mathbf{B}]$ . As the magnetic field perturbation in a low-beta plasma is negligibly small, one can neglect the l.h.s. in this equation thereby arriving at the equation

$$\nabla \times [\boldsymbol{\xi} \times \mathbf{B}] = 0. \quad (11)$$

It shows that the cross-product inside the square brackets has to be a gradient of some scalar function. We use the following representation:

$$\boldsymbol{\xi} \times \mathbf{B} = \frac{ic}{\omega} \nabla \delta \varphi. \quad (12)$$

The coefficient in front of the gradient is chosen so as to make obvious that  $\delta \varphi$  is the potential perturbation. This equation also shows that  $\delta \varphi$  is constant along the field lines,

$$\mathbf{t} \cdot \nabla \delta \varphi = 0. \quad (13)$$

Equation (12) yields the following expression for the normal component of the displacement:

$$\xi_{\perp} = \frac{ic}{\omega B^2} \mathbf{B} \times \nabla \delta \varphi. \quad (14)$$

If one ‘‘paints’’ a certain field line and finds displacements described by Eq. (14) for every point on this line, one discovers that the new line is also a field line of an unperturbed magnetic field (Fig. 3). The fact that perturbations are strongly elongated in the axial direction is a reason why this mode is called ‘‘the flute mode.’’

Equations (9) and (10) allow one to find the perpendicular component of the current perturbation:

$$\delta \mathbf{j}_{\perp} = \frac{c}{B^2} \left\{ -\omega^2 \rho \mathbf{B} \times \boldsymbol{\xi} + \mathbf{B} \times \nabla \delta p_{\perp} + (\delta p_{\parallel} - \delta p_{\perp}) \times [\mathbf{B} \times (\mathbf{t} \cdot \nabla) \mathbf{t}] - \mathbf{B} \times \delta \mathbf{f}_{add} \right\}. \quad (15)$$

The current is divergence-free; this allows one to relate the parallel and perpendicular currents:  $B \partial (\delta j_{\parallel} / B) / \partial \ell + \nabla \cdot \delta \mathbf{j}_{\perp} = 0$ . By integrating this equation along the field line between the end plates, one finds

$$\frac{\delta j_{\parallel 1}}{B_1} - \frac{\delta j_{\parallel 2}}{B_2} = \int_{r_1}^{r_2} \frac{d\ell \nabla \cdot \delta \mathbf{j}_{\perp}}{B}. \quad (16)$$

Here, the symbols ‘‘1’’ and ‘‘2’’ refer to two ends of the flux tube. This equation is a source of a number of results for a broad variety of settings, and we will use it in the subsequent sections. In particular, if the walls are non-conducting or if the ends of the plasma column are separated from the walls by a very low-density, poorly conducting plasma, the left-hand side becomes zero.

Using standard equations of vector analysis, the fact that the magnetic field is curl-free, and the constancy of  $\delta \varphi$  along the field line, one finds that (Appendix A)

$$\nabla \cdot \delta \mathbf{j}_{\perp} = ic^2 \omega \nabla \cdot \left( \frac{\rho \nabla \delta \varphi}{B^2} \right) + \frac{c}{B^2 r} \frac{\partial B}{\partial n} \frac{\partial (\delta p_{\perp} + \delta p_{\parallel})}{\partial \vartheta} - c \nabla \cdot \frac{\mathbf{B} \times \delta \mathbf{f}_{add}}{B^2}. \quad (17)$$

The first term in right-hand side describes the inertial effects, whereas the second term describes the instability drive. As it is proportional to the curvature  $\kappa$  (Eq. (6)), one can say that we are dealing with the curvature-driven instability. The third term describes possible effects of additional forces.

## B. Paraxial mirror

Consider a situation where the plasma occupies a region near the magnetic axis, at the radii  $r$  much smaller than the characteristic scale of the axial variation of the magnetic field  $L$ , i.e., the parameter

$$\varepsilon \equiv r/L \quad (18)$$

is much smaller than 1. This situation is of a significant practical importance, as the length of a mirror is typically much larger than its radius (Table I).

In the paraxial region, the magnetic field strength  $B$  is equal to the field on axis up to the terms of the second order in  $r$  (an expansion to the higher-order terms can be found in Ref. 27). In the paraxial approximation, neglecting terms  $\sim \varepsilon^2$ , one has

$$d\ell = dz, B = B(z), \quad \rho = \rho(\Psi, z). \quad (19)$$

The magnetic flux can, therefore, be approximately presented as

$$2\pi \Psi \approx \pi B r^2, \quad (20)$$

with  $B$  being the magnetic field on axis. The equation for the flux surface  $\Psi = \text{const}$  is just

$$r(z) = \sqrt{\frac{2\Psi}{B(z)}} \quad (21)$$

and the curvature in the same approximation is

$$\kappa = r'' = -\sqrt{\frac{\Psi}{2}} \left( \frac{B'}{B^{3/2}} \right)', \quad (22)$$

where primes denote the differentiation with respect to  $z$ .

The paraxial approximation allows for substantial simplifications in Eq. (17). We start from the first term, containing derivatives of the potential  $\delta \varphi$ . We ignore here all the terms containing the first and higher derivatives over  $z$  and obtain the following simplified expression

$$\nabla \cdot \left( \frac{\rho \nabla \delta \varphi}{B^2} \right) \approx \frac{2}{B} \left[ \frac{\partial}{\partial \Psi} \left( \rho \Psi \frac{\partial \delta \varphi}{\partial \Psi} \right) - \frac{\rho m^2 \delta \varphi}{4\Psi} \right]. \quad (23)$$

When deriving the last term, we explicitly used the  $\exp(im\vartheta)$  structure of the perturbations.

The normal to the field line approximately coincides with the radial direction, and the normal displacement can be approximately identified with the radial displacement. Therefore, when a flux tube is displaced in the radial or azimuthal direction, the plasma filling this tube is merely advected together with the fluxtube. Axial forces driven by the tube displacement are negligibly small (as the curvature of the tube

is small) and do not cause any plasma redistribution along the tube. This allows us to use a very simple expression for the pressure perturbation

$$\delta p_{\perp} + \delta p_{\parallel} \approx -\xi_n \frac{\partial}{\partial n} (p_{\perp} + p_{\parallel}) = -\frac{mc}{\omega} \delta\varphi \frac{\partial}{\partial \Psi} (p_{\perp} + p_{\parallel}). \quad (24)$$

We used here Eqs. (7) and (14). With this observation made and with Eq. (17) taken into account, one can present the integral (16) as

$$\frac{i\omega}{c^2} \left( \frac{\delta j_{\parallel 1}}{B_1} - \frac{\delta j_{\parallel 2}}{B_2} \right) = \omega^2 \left[ 4 \frac{\partial}{\partial \Psi} \left( I \Psi \frac{\partial \delta\varphi}{\partial \Psi} \right) - I \frac{m^2 \delta\varphi}{\Psi} \right] - m^2 \delta\varphi D, \quad (25)$$

where  $I$  is related to the inertia of the plasma and  $D$  is related to the instability drive

$$I(\Phi) = \int_{\Psi_1}^{\Psi_2} \frac{\rho(\Psi, z) dz}{2B^2(z)}, \quad (26)$$

$$D(\Psi) = \int_{\Psi_1}^{\Psi_2} \frac{\kappa(\Psi, z) dz}{r(\Psi, z) B^2(z)} \frac{\partial}{\partial \Psi} [p_{\parallel}(\Psi, z) + p_{\perp}(\Psi, z)].$$

We recall that, according to Eq. (13),  $\delta\varphi$  in Eq. (25) depends only on  $\Psi$ , with the  $\exp(im\vartheta)$  dependence on  $\vartheta$  already folded into analysis. Note also that these results hold for both collisionless plasmas, with the equilibrium pressure tensor determined by solution of a kinetic equation, and for a collisional plasma, where the pressure and flow velocity along the field lines are determined by solving hydrodynamic equations. Note that the parallel momentum flux  $p_{\parallel}$  contains both thermal pressure and ram pressure  $\rho v^2$ , with  $v$  being the parallel flow velocity.

Consider the case where there are no currents emanated from the ends of the fluxtube. Multiplying the r.h.s. of Eq. (25) by  $\delta\varphi^*$  and integrating over  $\Psi$  from the axis to the radius well outside the plasma, one obtains then that  $\omega^2$  is real,

$$\omega^2 = -m^2 \left( \int D |\delta\varphi|^2 d\Psi \right) \left[ \int 4I\Psi |\partial\delta\varphi/\partial\Psi|^2 d\Psi + m^2 \int I |\delta\varphi|^2 d\Psi / \Psi \right]^{-1}, \quad (27)$$

as it should be, based on the energy principle for a non-dissipative plasma.<sup>28</sup> The change of the sign of the first term in the denominator compared to its sign in Eq. (25) occurred due to the integration by parts. Note that the integral of  $|\delta\varphi|^2/\Psi$  converges, as regular solutions for  $\delta\varphi$  tend to zero at the origin. The numerator represents the drive, whereas the denominator represents the inertia. The fastest growing modes correspond to large mode numbers  $m$ , for which one can neglect the first term in the denominator.

A qualitative explanation is as follows: If one considers a thin flux tube undergoing a radial displacement, the fast growth would favor a tube with a cross-section similar to a cross-section of a ribbon (i.e., much thinner azimuthally than radially,  $m \gg 1$ , Fig. 3(b)). When such fluxtube moves radially, it causes only minor displacements of a plasma around

it, so that the inertia is limited to that of the plasma occupying the fluxtube itself. Quantitatively, this can be expressed as a statement of a small ‘‘induced mass’’ (Ref. 29, p. 28). The approach based on the analysis of these ‘‘ribbon-like’’ perturbations can be used to find the growth-rate of the fastest growing perturbations without resorting to a decomposition in the azimuthal angle. This was done for the GDT in Ref. 30.

A Lagrangian approach to the paraxial stability was developed in Refs. 31–35. In addition to a pure MHD stability, it allows one to describe such effects as a slow plasma rotation, finite Larmor radius effects, and ballooning effects. A summary of these analyses, together with a brief description of the initial-value code (FLORA) based on them is presented in Appendix B.

For perturbations with  $\xi$  localized near some flux surface  $\Psi = \Psi_0$  and having the aforementioned ‘‘ribbon-like’’ shape, one can both neglect the first term in the denominator and also pull the terms  $D$  and  $I/\Psi$  out of the integrals, thereby obtaining the following expression for the growth-rate of localized modes:

$$\omega^2 = -(\Psi D/I)_{\Psi=\Psi_0}. \quad (28)$$

In order for a given equilibrium state be stable,  $D$  has to be negative on every flux surface (at every  $\Psi_0$ ). This is a necessary condition for the stability of a given configuration; according to Eq. (27), it is also sufficient.

Assume now that the plasma is unstable and has a smooth radial density profile, with a characteristic radius  $a$  in the equatorial plane. If the magnetic field increases smoothly, over the whole length of the device, from the minimum in the equatorial plane to the maximum in mirrors, the field-line curvature can be estimated as  $a/L^2$ . On the other hand, the ratio of pressure to the density is equal, by the order of magnitude, to the square of the sound speed. In mirrors, the ions are usually warmer than electrons, and the sound speed can be estimated as the ion thermal speed  $v_{Ti}$ . Then, the ratio— $\Psi D/I$  in Eq. (28) can be estimated as— $v_{Ti}^2/L^2$ , yielding the following estimate for the characteristic growth-rate  $\Gamma_0$ :

$$\Gamma_0 \sim \frac{v_{Ti}}{L}. \quad (29)$$

If the mirror machine is made of a long solenoid with short mirror sections (of the length  $L_I$  satisfying  $a < L_I \ll L$ ), then the contribution to inertia ( $I$ ) comes from the long solenoid, whereas the contribution to the drive comes mostly from the short end sections. This leads to a larger growth-rate,  $\Gamma_0 \sim v_{Ti}/\sqrt{L_1 L}$ . For a given length of a mirror zone  $L_I$ , there exists an optimum dependence of  $B(z)$  in this zone, the one that makes the growth rate minimally possible for given length constraints. Numerically, the growth rates are quite large (see last column of Table I). If left un-inhibited, the instability would lead to the loss of the plasma within several ion transit times, i.e., within the same time as the free axial expansion time of a cylindrical plasma without any axial confinement.

One can note that the paraxial approximation leads to significant simplifications in the analyses of the finite- $\beta$  effects.

In particular, in the radial equilibrium condition (5), the second term contains a small parameter  $\varepsilon^2$  (Eq. (18)) compared to the first. The equilibrium condition then becomes simply

$$\frac{B^2}{8\pi} + p_{\perp}(\Psi, z) = \frac{B_{vac}^2(\Psi, z)}{8\pi}. \quad (30)$$

### C. Plasma with a sharp boundary

As was stated in Sec. III B, the necessary and sufficient condition for stability in the paraxial approximation is the negativity of  $D$  (Eq. (26)). It has to be negative on all flux surfaces, as otherwise one would be able to create a perturbation of  $\varphi$  localized near the surface where  $D$  is positive and make  $\omega^2$  negative, signifying the instability (and thereby inaccessibility of the assumed configuration).

For the case of the plasma with a sharp boundary (within which the plasma is radially uniform), the derivative over the flux is very large at the boundary,  $-(p_{\parallel} + p_{\perp})/\Delta\Psi$ , where  $p_{\parallel}$  and  $p_{\perp}$  are taken inside the (radially uniform) plasma, and  $\Delta\Psi$  is a small width of the transition zone. In this case, the stability of the boundary is a concern. The stability condition can be written as

$$\int_{z_1}^{z_2} \frac{a''(z) [p_{\parallel}(z) + p_{\perp}(z)] dz}{a(z)B^2(z)} > 0, \quad (31)$$

where the integration is extended to the points where the plasma pressure is negligible or to the non-conducting end walls;  $a(z)$  is the radius of the plasma boundary. This condition is called “a pressure-weighted curvature” condition. It is sometimes (incorrectly) characterized as the general stability condition. In reality, it relates only to a special case of a sharp boundary. On the other hand, it allows for a quick assessment of various factors affecting the plasma stability and, therefore, indeed deserves some attention. Another form of the stability condition (31) that uses the relation  $B = \text{const}/a^2$  (valid in the paraxial approximation) is

$$J \equiv \int_{z_1}^{z_2} a^3(z)a''(z) [p_{\parallel}(z) + p_{\perp}(z)] dz > 0. \quad (32)$$

This condition was applied, in particular, to the analysis of the stability of GDT,<sup>30</sup> of the stabilization technique based on the use of the sloshing ions,<sup>36</sup> and of the kinetic stabilizer.<sup>37–40</sup> What is obvious from Eq. (32) is that the contribution of areas of weak magnetic field (large plasma radii) is strongly emphasized by the presence of the  $a^3$  factor.

In some cases, the mirror-trapped plasma can be considered as isotropic. In particular, this can be realized in a mirror with a very high mirror ratio, so that the loss cone is very narrow. Near the mirror throats, the pressure becomes anisotropic, but the factor  $a^3$  is so small that the contribution of this zone is negligible. For the isotropic plasma, the pressure is uniform along  $z$  and the stability criterion (32) becomes

$$\int_{z_1}^{z_2} a^3(z)a''(z) dz > 0, \quad (33)$$

where the integration is performed between the field maxima. However, integrating by parts, one finds that this integral is always negative,

$$\int_{z_1}^{z_2} a^3(z)a''(z) dz = -3 \int_{z_1}^{z_2} a^2(z)[a'(z)]^2 dz < 0, \quad (34)$$

meaning instability. The source of this problem is that, in the standard mirror layout of Figs. 1 and 3, the unfavorable curvature corresponds to large plasma radii and is therefore emphasized in the instability criterion.

A related interpretation can be formulated in terms of a specific volume of flux tubes,

$$U \equiv \int \frac{dl}{B}, \quad (35)$$

with integration between strong mirrors. Using Eqs. (34) and (8), which, in the paraxial approximation, yields  $a'' = -aB^2\partial[1/B(\Psi, z)]/\partial\Psi$ ; one sees that, for stability, the function  $U(\Psi)$  should be a decreasing function, whereas in the paraxial domain, it is an increasing function.

In the sharp-boundary model, the unstable perturbations are localized near the plasma boundary; for large  $m$ , the radial scale of the localization is  $\sim a/m$ . The evaluation of the integrals  $D$  and  $I$  in Eq. (26) yields in this case a growth-rate  $\sim \sqrt{m}\Gamma_0$  (we assume  $m > 0$ ). This is quite similar to a familiar Rayleigh-Taylor instability—an analogy emphasized by Rosenbluth and Longmire.

These results are based on a simple and robust description and have been re-derived by several techniques since the first publication by Rosenbluth and Longmire.<sup>26</sup> Together with the failure of some initial experiments with axisymmetric mirrors (like that described in Ref. 23), this led to attempts to make mirrors stable by making them non-axisymmetric. This was successfully accomplished in the form of so-called “Ioffe bars”<sup>5</sup> and led to the outstanding results in the already mentioned 2XIB experiments,<sup>6–8</sup> where MHD-stable plasma with beta close to 1 was achieved in a so-called Yin-Yang geometry with a quadrupole symmetry.

On the other hand, the conclusion encapsulated in Eq. (34) was reached with several significant assumptions. First, it assumes an isotropy of the plasma. Second, it is based on the sharp-boundary model. Third, it is based on the paraxial expansion. Fourth, it ignores the role of the escaping plasma in the end tanks. Getting rid of any of these assumptions may, in fact, lead to axisymmetric stability even within the framework of pure MHD (i.e., without bringing up new effects, like FLR, or plasma rotation, or something more exotic).

Note also that the stability is determined by some type of averaging along the field line. This may allow one to connect several pieces of an axisymmetric mirror system, some of which, taken separately, are unstable, whereas the others are stable, so that the overall system would be stable. In this case, the stabilizing elements are called “the anchors.”

## IV. FLR EFFECT

The instability drive is proportional to the field-line curvature,  $a''$ , and decreases as  $1/L^2$  in a long-thin mirror. In

such a situation, other terms, which are small at first sight, may actually become important. In particular, as was noted in a classic paper by Rosenbluth, Krall, and Rostoker,<sup>41</sup> the effects associated with the finiteness of the ion Larmor radius  $\rho_i$  may become dominant, despite the fact that the ratio  $\rho_i/a$  is small. To evaluate the FLR effect, one has to add viscous terms to the momentum flux tensor. [This way of deriving the FLR effect was suggested in Refs. 42 and 43.] For long-thin flux tubes, only components perpendicular to  $z$  are important. Of those, the largest ones are the gyro-viscous terms, which are proportional to  $\rho_i$  in the first power. The further analysis is simplified in that one can evaluate these terms neglecting the field line curvature, which would bring up an additional small factor of  $(a/L)^2$  to the FLR contribution, making it decisively smaller than the curvature drive. Then, the contribution of  $\delta f_{add}^{(v)}$  (with the superscript “v” referring to viscosity) to the divergence of the cross-field current in Eq. (16) becomes simply

$$\nabla \cdot \delta \mathbf{j}_\perp = \dots + \frac{c}{B_z} \left( \nabla \times \mathbf{f}_{add}^{(v)} \right)_z, \quad (36)$$

where the dots represent other terms in the r.h.s. of Eq. (17). The presence of  $\delta f_{add}^{(v)}$  leads to the change of expression (25) for parallel currents and thereby affects the dispersion relation (28) corresponding to zero currents at the ends. The resulting dispersion relation accounting for the FLR effects for short-wavelength modes ( $m > 1$ ) can be schematically presented as (Cf. Ref. 41)

$$\omega^2 + m\omega(v_{Ti}\rho_i/a^2) + \Gamma_0^2 = 0, \quad (37)$$

where  $\Gamma_0$  is given by Eq. (29). We have written Eq. (37) assuming that, in the absence of the gyroviscosity, the system is unstable,  $\Gamma_0^2 > 0$ . The stabilizing effect comes from the second term and is obviously related to the finiteness of the ion Larmor radius. One should remember<sup>41</sup> that, for  $m = 1$ , the stabilizing term disappears (see below in this section).

We see that the stabilization occurs if  $m\rho_i L/2 > a^2$ . In other words, significant FLR effects appear if the dimensionless parameter  $(m/2)F_{FLR}$ , with

$$F_{FLR} \equiv \frac{\rho_i L}{a^2}, \quad (38)$$

is greater than 1. This condition is satisfied for a variety of mirror systems (see Table II).

TABLE II. FLR effect for devices listed in Table I.<sup>a</sup>

Device type	$\rho_i$ , cm	$L/a$	$a/\rho_i$	$F_{FLR}$
GDT device	1 (6)	90	8 (1.3)	12 (70)
Neutron source	0.3 (2.3)	80	50 (6)	1.6 (12)
Hybrid driver	1.3	80	40	2
Pure fusion	1	150	100	1.5

<sup>a</sup>Notation:  $\rho_i$  – the ion gyro-radius; other symbols are the same as in Table I. The parameter  $F_{FLR}$  is defined by Eq. (38); the larger this parameter, the stronger the FLR effects. The number in parentheses correspond to the hot ion component.

It is worthwhile to note that the original paper by Rosenbluth, Krall, and Rostoker<sup>41</sup> dealt with the stability of a mirror plasma with a sharp boundary, and the last term in the analog of Eq. (37) (Eq. (37) of Ref. 41 with  $W = 0$ ) was  $m\Gamma_0^2$  (see Sec. III). We are considering here the case of a plasma with smooth radial distribution of parameters, more in the spirit of Refs. 35, 42 and 43.

As was already mentioned, there is an important case which is not covered by Eq. (37) that of the  $m = 1$  mode of a global lateral displacement of the plasma column. Indeed, the viscous effects (including gyro-viscous effects) are important only if relative motion of the flux tubes is present. However, for the mode of a global lateral displacement, in which the column moves as a whole, the viscous effects disappear and the instability is recovered. Obviously, the global displacement mode with  $\xi_\perp = const$  over the plasma cross-section corresponds in the paraxial approximation to  $m = 1$  and the radial potential perturbation proportional to  $r$  (so that the electric field is uniform over the cross-section, see Eq. (12) and Ref. 41). Consider, for example, a uniform displacement in the  $y$  direction, so that the potential is a linear function of  $x$ . Recalling that the potential is constant along the field lines, one can say that the potential has the form

$$\delta\varphi = const \cdot x\sqrt{B_z}. \quad (39)$$

The displacement  $\xi$  corresponding to this potential is

$$\xi_y = const \frac{ic}{\omega\sqrt{B_z}}. \quad (40)$$

Next, we note that, as the viscous force is an internal force acting between the fluid elements, one has in the paraxial approximation

$$\int \delta f_{add\perp}^{(v)} dS = 0, \quad (41)$$

where the integration is performed over a plane perpendicular to the axis  $z$ . [One can check Eq. (41) also directly, by using explicit expressions for the viscous force from Ref. 44.] The paraxial approximation is important here, as we assume that every segment of the plasma column can be approximated by a cylinder; any corrections contain an additional small factor of order of  $(a/L)$  or higher. One can see that, by multiplying the r.h.s. of Eq. (38) by this small factor, one would automatically reverse the inequality  $F_{FLR} > 1$ , this meaning that corrections of this order in the FLR problem can be neglected.

A more complex system, where the plasma with strong FLR effects is in a lateral contact with a cold plasma line-tied to the end walls was considered in Ref. 45. We do not consider here a situation where the FLR effects are strong in the inner part of the plasma cross-section and weak in the outer part.

For perturbations described by Eqs. (39) and (40), Eqs. (24) and (17) in the paraxial approximation yield

$$\begin{aligned} \delta p_\perp + \delta p_\parallel &= \xi_y \sin\vartheta \frac{\partial(p_\perp + p_\parallel)}{\partial r} \\ &= const \frac{ic \sin\vartheta}{\omega\sqrt{B}} \frac{\partial(p_\perp + p_\parallel)}{\partial r}; \end{aligned} \quad (42)$$

$$\begin{aligned} \nabla \cdot \delta \mathbf{j}_\perp = & \text{const} \frac{ic^2 \omega \cos \vartheta}{B^{3/2}} \frac{\partial \rho}{\partial r} - \frac{c\kappa}{Br} \frac{\partial}{\partial \vartheta} (\delta p_\perp + \delta p_\parallel) \\ & - \frac{c}{B} \nabla \cdot \left[ \hat{z} \times \delta \mathbf{f}_{add\perp}^{(v)} \right]. \end{aligned} \quad (43)$$

For the case of strong FLR effects, when condition  $F_{FLR} > 1$  holds by significant margin, the last term in Eq. (43) is much larger than the other two. To eliminate it, we multiply Eq. (43) by  $x$  and integrate it over the  $xy$  cross sections. We note that, for an arbitrary 2D vector  $\mathbf{C}_\perp$  that decreases rapidly enough at large distances from the axis, one has

$$\int x(\nabla \cdot \mathbf{C}_\perp) dS = - \int C_x dS. \quad (44)$$

When applied to the last term in Eq. (43), this condition yields (see Eq. (41))

$$\int x \nabla \cdot \left[ \hat{z} \times \delta \mathbf{f}_{add\perp}^{(v)} \right] dS = - \hat{y} \cdot \int \delta \mathbf{f}_{add\perp}^{(v)} dS = 0. \quad (45)$$

Equation (45) is a solubility condition that eliminates the terms that contain an explicitly large parameter related to the gyroviscosity. With this notion, and using Eqs. (42), (43), we obtain in the paraxial approximation:

$$\begin{aligned} \int x(\nabla \cdot \delta \mathbf{j}_\perp) dS = & \text{const} \times ic^2 \left[ \frac{\omega}{B^{5/2}} \int \rho d\Psi \right. \\ & \left. - \frac{1}{\omega B^2} \frac{d^2}{dz^2} \left( \frac{1}{\sqrt{B}} \right) \int (p_\parallel + p_\perp) d\Psi \right]. \end{aligned} \quad (46)$$

Instead of Eq. (25), we have now

$$\begin{aligned} \frac{i\omega}{c^2} \left( \frac{1}{B_1} \int x \delta j_{\parallel 1} dS - \frac{1}{B_2} \int x \delta j_{\parallel 1} dS \right) \\ = \text{const} \left[ \omega^2 \int \left( \frac{1}{B^{7/2}} \int \rho d\Psi \right) dz \right. \\ \left. - \int \left( \frac{1}{B^3} \frac{d^2}{dz^2} \left( \frac{1}{\sqrt{B}} \right) \int (p_\parallel + p_\perp) d\Psi \right) dz \right]. \end{aligned} \quad (47)$$

For the case where the current to the end walls is zero, one obtains a dispersion relation analogous to Eq. (28)

$$\omega^2 = -D_G/I_G \equiv -\Gamma_G^2, \quad (48)$$

where

$$\begin{aligned} D_G = & - \int \left( \frac{1}{B^3} \frac{d^2}{dz^2} \left( \frac{1}{\sqrt{B}} \right) \int (p_\parallel + p_\perp) d\Psi \right) dz; \\ I_G = & \int \left( \frac{1}{B^{7/2}} \int \rho d\Psi \right) dz \end{aligned} \quad (49)$$

and the subscript ‘‘G’’ refers to the global mode. The curvature drive enters via derivatives of the magnetic field strength. Note that the powers of the magnetic field that enter Eq. (49) are different than those that enter Eq. (26): the zone of the weak field makes a larger contribution to both integrals. This is related to a different structure of Eq. (47), where the global mode ‘‘samples’’ the whole cross-section of the plasma, with the potential varying linearly with the radius. This leads to a stronger contribution of the weaker

fields to the stability integral  $D_G$ . We return to this issue in Secs. IV A and V.

Expression (49) for the drive contains the plasma pressure integrated over the cross-section and leads to a softer stability condition than Eq. (28); in particular, even the profiles which are unstable in a certain range of radii according to Eq. (28) can be stable with respect to the global mode. On the other hand, in a simple axisymmetric mirror machine with a high mirror ratio, the plasma remains unstable, with the growth-rate being of the same order of magnitude as Eq. (29).

## V. STABILIZATION BY THE FAVORABLE CURVATURE

### A. Using expanding magnetic field in the end tanks

Plasma lost through the ends of a mirror device and flowing to the end-plates may stabilize the device if the field lines in the end-tank have a large-enough favorable curvature, as shown in Fig. 4. In order for this stabilizing effect to be significant, the amount of plasma lost through the ends must be not-too-small (see below).

Due to a rapid decrease of the magnetic field between the mirror and the end wall, the perpendicular energy of the ions is converted into their parallel energy; in addition, the ions are accelerated by the ambipolar electric field, which provides the plasma neutrality. As the ambipolar potential depends only logarithmically on the density ratio, one can roughly approximate the ion expansion as a flow with some constant ion energy  $W_i$ , where  $W_i$  somewhat exceeds the thermal energy of both electrons and ions. The plasma density in this constant-velocity flow scales as  $B$ , and the parallel momentum flux  $p_\parallel \approx \rho v^2 = 2m_i n W_i$  also scales as  $B$  [note that the quantity  $\rho v^2$  is sometimes called ‘‘ram pressure’’]. Taking as a reference point the field at the end wall, one can write

$$p_\parallel \approx p_{\parallel \text{wall}} (B/B_{\text{wall}}). \quad (50)$$

This approximation becomes reasonably accurate at some distance from the mirror, where the magnetic field decreases by more than a factor of  $\sim 2$  compared to the mirror field. We will see that the vicinity of the mirror does not contribute significantly to the stability integral, so that the exact dependence of  $p_\parallel$  vs.  $B$  near the mirror is unimportant.

We will consider stability in the model with the sharp plasma boundary (Sec. III C) and base our further analysis on Eq. (32). We split the stability integral  $J$  into the contribution of the confinement region (which we assume to be negative) and of the two end tanks, so that  $J = J_{\text{conf}} + 2J_{\text{end}}$ . According to discussion of Sec. III C,

$$|J_{\text{conf}}| = 2p_0 \int a^3(z) a''(z) dz \sim 4p_0 a_0^4/L, \quad (51)$$

where  $p_0$  is the pressure of an almost isotropic plasma confined between strong mirrors.

To evaluate  $J_{\text{end}}$ , we take a power-law dependence of the plasma radius vs. the distance  $z$  from the mirror,  $a = a_{\text{wall}}(z/L_{\text{end}})^\alpha$ , where  $L_{\text{end}}$  is the length of the end tank (the distance between the mirror and the wall). This

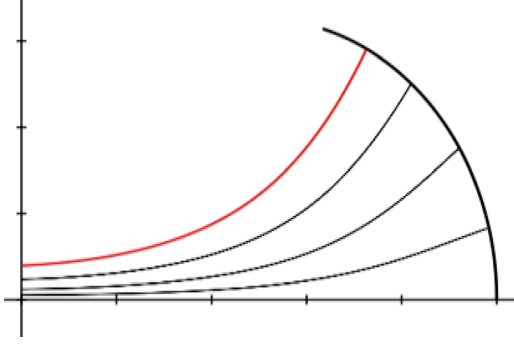


FIG. 4. (Color online) Flaring of the magnetic field lines in the end tank. The mirror throat is at  $z=0$ , the confinement zone (not shown) is at  $z < 0$ . Note the favorable curvature of the magnetic field lines. Highlighted is a limiting flux surface  $a(z)$ .

dependence cannot be used in the immediate vicinity of the mirror but, as we will see below, the contribution of the mirror zone to the stability integral is very small, so that the exact dependence of  $a$  vs.  $z$  in this zone is unimportant. In order to have a favorable curvature of the field lines, one has to have  $\alpha > 1$ .

Taking into account that, according to Eq. (50),  $p_{||} \approx p_{||wall}(a_{wall}/a)^2$ , one finds that

$$J_{end} = \frac{\alpha(\alpha-1)a_{wall}^4 p_{||wall}}{L_{end}} \int_0^1 \left(\frac{z}{L_{end}}\right)^{2(\alpha-1)} d\left(\frac{z}{L_{end}}\right) = \frac{\alpha(\alpha-1)a_{wall}^4 p_{||wall}}{(2\alpha-1)L_{end}}. \quad (52)$$

It is possible to relate  $J_{conf}$  and  $J_{end}$  via the energy confinement time  $\tau_E$  in the mirror machine. Indeed, the energy stored in the confinement zone is approximately equal to  $(3p_0/2)\pi a_0^2 L$ . The energy lost through two ends per unit time is approximately  $p_{||wall}\sqrt{W_i/2m_i}\pi a_{wall}^2$ . The energy confinement time  $\tau_E$  is the ratio of the first to the second, i.e.,

$$p_{||wall} = p_0(a_0^2/a_{wall}^2)(3L/2\tau_E\sqrt{2W_i/m_i}). \quad (53)$$

With this notion, one can write the following stability condition ( $2J_{end} > J_{conf}$ ):

$$F_{end} \equiv \frac{4\alpha(\alpha-1)}{3(2\alpha-1)} \frac{L^2}{\tau_E L_{end} \sqrt{2W_i/m_i}} \left(\frac{a_{wall}}{a_0}\right)^2 > 1. \quad (54)$$

One sees that this stability criterion favors long devices and/or short confinement times. Condition (54) can be met in a 2-3 km long fusion reactor based on a confinement of a collisional plasma<sup>14</sup> (where  $F_{end}$  is large due to a large  $L$ ) and in mirror-based neutron sources<sup>16,17</sup> (where  $F_{end}$  is large due to a small  $\tau_E$ ).

In a collisional plasma of a gas-dynamic trap,  $\tau_E \sim LR/\sqrt{2W_i/m_i}$ , where  $R$  is the mirror ratio. Assuming that  $\alpha = 3/2$ , one finds from Eq. (54), the following stability criterion:  $R < 0.12(a_{wall}/a_0)^2(L/L_{end})$ . For  $a_{wall}/a_0 \sim 5$  and  $L/L_{end} \sim 5$ , one finds that the stability can be provided at  $R < 30$ , in a reasonable agreement with experimental results corresponding to early experiments on the gas-dynamic trap, where the pressure was determined by the collisional compo-

nent.<sup>46</sup> However, for the devices with a large confinement time, for realistic assumptions regarding the diameter of the end tank, condition (54) is violated by a large margin. All this is illustrated in Table III, which shows the parameter  $F_{end}$  for the four devices of Table I.

There are constraints on the achievable degree of the flaring. One constraint is related to the use of the paraxial approximation. This approximation means that the angle between the magnetic axis and the limiting flux surface must be less than one, i.e.,  $a_{wall} < L_{end}/\alpha$ . Also, the ion gyroradius must be smaller than the field line curvature in the end tanks. We will not get into the further, device-specific, details of these constraints.

One more constraint stems from our assumption that the plasma pressure (including the ram pressure  $\rho v^2$ ) is small right to the end-wall. For very large expansion ratios, this condition can be violated. Indeed, according to Eq. (50), the ram pressure in the end-tanks scales as  $B$ , whereas the magnetic pressure scales as  $B^2$ , so that the second eventually may become smaller than the first. This would lead to violation of the flute model and to essential decoupling of perturbations in the downstream flow from those in the rest of the plasma. This issue is discussed in Ref. 30.

Equation (54) has to be modified in the case of a two-component plasma, where there is a fast component slowing down against colder collisional plasma, which determines the outflow. Such a situation will be met in a neutron source based on the gas-dynamic trap. In this case, instead of Eq. (51), one would have an equation

$$J_{conf} \sim 4(1+h)p_0 a_0^4/L, \quad (55)$$

where  $h$  is a relative contribution of the hot, mirror-confined component

$$h \equiv \frac{L}{4p_0 a_0^4} \left\{ \int_{z_1}^{z_2} a^3(z) a''(z) [p_{||hot}(z) + p_{\perp hot}(z)] dz \right\}. \quad (56)$$

Accordingly, instead of the stability condition (54), one would have  $F_{end} > 1+h$ , and  $\tau_E$  will be an energy confinement time of a colder collisional component. This consideration is folded into the numbers representing the neutron source in Table III.

One more comment is related to the mode of the global displacement, for which the integrations in the stability integral  $D_G$  strongly emphasize the contributions of the weak magnetic field. One could therefore anticipate a much

TABLE III. Effects of the end-tank stabilization for devices listed in Table I.<sup>a</sup>

Device type	$L_{end}$ (m)	$a_w, m$	$a_w/L_{end}$	$\sqrt{2W_i/m_i}$ m/s	$(a_w/a_0)^2$	$F_{END}$
GDT device	1.5	0.8	0.55	$1.7 \times 10^5$	100	3.3
Neutron source	3	3	1.0	$3.3 \times 10^5$	400	1
Hybrid driver	5	4	0.8	$10^6$	64	0.01
Pure fusion	10	10	1.0	$2 \times 10^6$	100	0.0003

<sup>a</sup>Notation:  $L_{end}$  – a distance between the mirror and the end-wall,  $a_w$  – plasma radius at the end-wall,  $W_i$  – the characteristic ion energy at the end wall, the parameter  $F_{END}$  defined by Eq. (54) characterizes the role of stabilization by the outflowing plasma; other parameters are the same as in Table I.

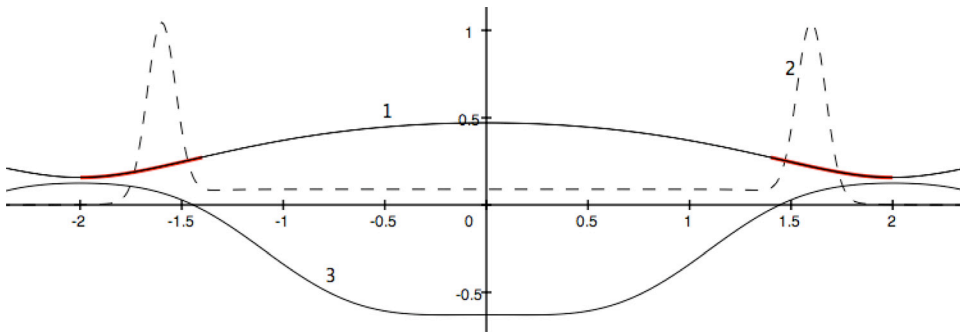


FIG. 5. (Color online) Stabilization with sloshing ions. Curve 1 shows the plasma boundary  $a(z)$ , curve 2 is a pressure  $p_{\parallel} + p_{\perp}$  of the sloshing ions with a narrow angular spread leading to a strong pressure peaking near the turning points; curve 3 is the product  $a^3 a'$ . All curves are in arbitrary units. The zones of favorable curvature are highlighted on curve 1.

stronger stabilizing effect of the end tanks on the global  $m = 1$  mode than on the local modes. However, for the global mode, the large parameter that enforces the plasma to move as a whole (in the transverse direction) is actually not so large (see Table II). The interplay of two effects, the FLR and the end-tank stabilization, makes the analysis more difficult. This more general analysis has not been performed thus far.

Instead of a funnel-like structure of the magnetic field in the end-tank, one can attach to the confinement zone a cusp cell, where the field line curvature is also favorable. Although the presence of the magnetic field null at the center of this cell does not allow filling it with confined plasma, the plasma flowing out from the confinement zone stays there for several transit times. Thus, its density becomes higher than in the case of just one transit, as in the expansion tanks, and the stabilizing contribution increases. This effect was demonstrated experimentally on the GDT facility.<sup>47</sup> A disadvantage of this approach is that it adds complexity to the overall design and, in reactor-scale facilities, creates an additional problem of spreading the energy flux escaping through the ring cusp.

## B. Stabilizing with sloshing ions

This stabilization technique has been first discussed by Hinton and Rosenbluth.<sup>36</sup> The idea is to inject ions not perpendicularly to the magnetic axis, but rather at some angle adjusted in such a way that the ion turning points would be situated in the areas of the favorable curvature (Fig. 5). Then, if the angular spread of the ions is small, a strong peaking of the function  $P \equiv p_{\parallel} + p_{\perp}$  will occur near the turning points, and one can hope that the integral (32) will be positive, meaning MHD stability. Note that the sloshing ion distributions have proven to be more stable with respect to velocity-space (loss-cone) instabilities than distributions produced by a normal injection.<sup>48–51</sup>

In the equilibrium,  $P$  is a function of the magnetic field strength,  $P = P(B)$ . On the other hand, as, in the paraxial approximation,  $B$  is related to  $a$  by  $B = \text{const}/a^2$ , one can consider  $P$  as a function of  $a$ . Having this in mind and performing an integration by parts in Eq. (32), one finds that

$$J = - \int (Pa^3)' a' dz = - \int a'^2 \frac{d(Pa^3)}{da} dz, \quad (57)$$

where prime means differentiation over  $z$ . This form of the stability integral shows that, in order to make the system sta-

ble, one has to create a situation where the product  $Pa^3$  would be a decreasing function of  $a$  at least at some  $a$ 's. The presence of a rapidly growing factor  $a^3$  makes this task quite difficult, meaning that  $P$  should decrease at some  $a$ 's faster than  $1/a^3$ . To fulfill this condition, one needs a small angular spread of the sloshing ions; this can be reached if the slowing-down of the ions by the electron drag is much faster than the ion-ion scattering, meaning that the injection energy should be much higher than the electron temperature. In Ref. 36, the required value of  $W_{inj}/T_e$  was found to be as high as 100. This does not seem practical for fusion energy applications, although may be of interest for mirror-based neutron sources. In Ref. 52, it was shown that, by optimizing the magnetic field profile and accentuating the favorable curvature region by making  $|a'|$  there large, one can reduce the required ratio  $W_{inj}/T_e$  to the values below 30, which are probably still too high for the fusion energy applications.

## C. Kinetic stabilizer

As seen from Eq. (32), the flute stability is most strongly affected by the areas of a weak magnetic field (the largest  $a$ 's). This circumstance makes the stabilizing contribution of the end-tank relatively large even at a relatively small plasma density in the expanders. Post<sup>37–40</sup> has noticed that one can further enhance this effect by creating a zone of a strong favorable curvature in the weak magnetic field of an expansion tank (Fig. 6) and injecting a stream of ions from the end-wall; the pitch-angle of these ions will be chosen so that they would be reflected back in the region of the favorable curvature, creating there a strong peak of the function  $P$  mentioned in Sec. V B. The fact that the magnetic field in this turning point will be quite small ( $a$  large) leads to a very strong enhancement of the stabilizing contribution and reduces requirements to the stabilizing ion stream. [The stream is, of course, neutralized by the electrons.]

One more possibility considered by Post<sup>38</sup> is to inject atomic particles into the zone of a strong favorable curvature in the end-tank (Fig. 7). The neutral particles, after been ionized and having initially a negligible energy, accelerate in the ambipolar electric field pushing them to the end-plate. Therefore, between the injection point and the end-plate, an ion flow with a finite parallel momentum flux is formed, and it contributes to the stabilization integral. The amount of gas injected has to be compatible with a constraint stemming from an inadmissibility of creating too many cold electrons in the expander.<sup>20</sup>

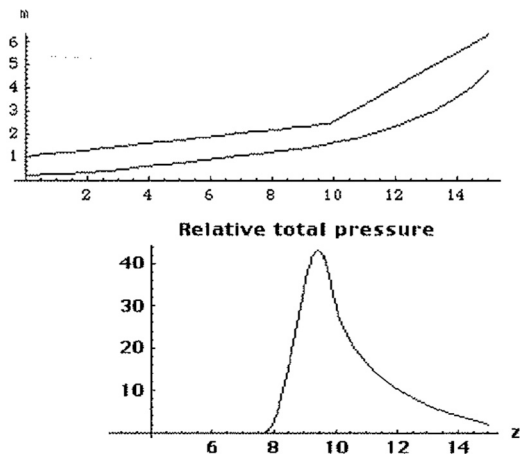


FIG. 6. Kinetic stabilizer. (a) Upper line: outline of coils in a “double-conical” expander; lower line: one of the field lines. (b) Pressure distribution of the stabilizing beam, with a sharp maximum in the optimum location. There is a need in the presence of the highly conducting plasma, connecting the stabilizer with the central part of the facility. Courtesy R.F. Post, Ref. 32.

In subsequent publications,<sup>39,40</sup> Post has also assessed the possibility of creating a pressure peak by other techniques, in particular, by a pulsed ECRH heating of the electrons in the desired point, with the repetition rate of the pulses being much higher than the expected growth rate of the instability.

#### D. Trapped particle modes

The kinetic stabilizer method, as well as stabilization by the outflowing plasmas, rely on the good electrical connection of the confinement zone (which, taken alone, is unstable in the case of an axisymmetric mirror) and a stabilizing element, which in both cases is situated in the end tank. The connection between the electrons in these two parts of the device is an issue of concern arising from the high electrostatic barrier and the high mirror ratio separating the two. The reason for concern is as follows.

In systems that are MHD flute stable, but where there is both stabilizing concave curvature and destabilizing convex curvature present, stability is achieved for MHD perturbations localized to the destabilization region by the additional magnetic energy that is induced due to the localization of the

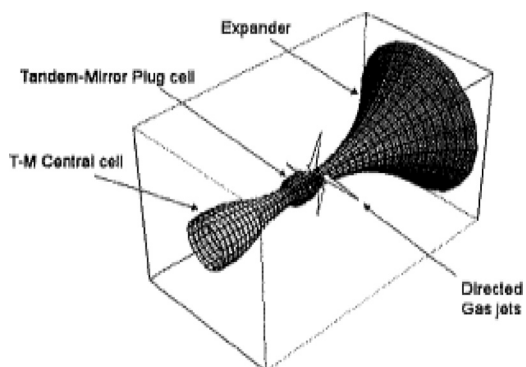


FIG. 7. Schematic of the end section of a tandem mirror, with gas injected in the expander where the field lines have a large favorable curvature. Courtesy R.F. Post, Ref. 32.

mode. However, as the flute mode at low beta is a pure electrostatic perturbation, it is prone to instability of spatially localized electrostatic perturbations in the destabilizing region that does not induce the stabilizing magnetic bending energy. This type of instability was first identified in tokamaks,<sup>53</sup> where there exist particles magnetically trapped on the outboard side of the tokamak where the unfavorable curvature induces a flute-like destabilizing response from the mirror trapped particles there. The passing particles, which feel a sinusoidal-like electrostatic perturbation, considerably reduce the instability growth rate from that expected from MHD theory. A similar type of effect takes place in a tandem mirror as well<sup>54,55</sup> where an electrostatic perturbation is localized to the central cell where the curvature is convex, thus destabilizing. The instability appears more vociferous than in a tokamak, as in the tandem mirror most of the plasma is trapped in the bad curvature region, so that the reduction in growth rate is considerably less than in a tokamak. There is even the possibility of the growth rate being as large as the MHD prediction.

The principal method of stabilization of the trapped particle mode is based on a property of orbits in a tandem mirror that is not readily achieved in a tokamak. That is, in a tandem, there is a large variation of the equilibrium electrostatic potential that produces different equilibrium orbits for electrons and ions. The result is that there is a different  $\mathbf{E} \times \mathbf{B}$  response to an electrostatic perturbation from electrons and ions that leads to charge uncovering in a manner similar to the FLR stabilization effect (Sec. IV). For example in the kinetic stabilizer, all the ions leaving the central cell are lost, while most of the electrons leaving the central cell region reflect back by an ambipolar potential formed to keep the ion and electron densities equal. This effect forces the trapped particle perturbation to oscillate at a finite frequency, which would stabilize the mode when this (radian) frequency exceeds twice the MHD growth rate. In the case where collisions are negligible, a necessary condition for stability for a displacement mode has recently been found as:<sup>56</sup>  $\langle n_{ct}/n \rangle (T_{eks}/8W_0) > M_{ks}$ , where  $\langle n_{ct}/n \rangle$  is the fraction of all the electrons in the kinetic stabilizer region that return to the central cell,  $M_{ks}$  is the ratio of the central cell flute drive to the stabilizing effect of the kinetic stabilizer,  $T_{eks}$  is the electron temperature in the kinetic stabilizer region, and  $W_0$  is the energy of the kinetic stabilizer beam. There is a concern of being able to meet this condition while simultaneously limiting the power that is needed to operate the kinetic stabilizer.

In Refs. 57 and 58, the role of electron collisions were accounted for. In Ref. 59, the instability was considered for the specific case of the gas-dynamic trap. Generally, trapped particle modes become slower when the electron temperature is low. The potential variation then decreases, and the residual instability—if any—becomes quite slow. However, if the electron temperature becomes too low, parallel electric resistivity may come into play and cause the appearance of so called “resistive ballooning” modes.

Experimentally, an identification of the collisionless trapped particle mode in the mirror geometry was made in Ref. 60. However, much more experimental data are

needed to confirm the theory and evaluate its nonlinear consequences.

Basically, all the stabilization techniques considered above have to be checked with respect to their vulnerability to the trapped particle modes. This has not been done yet; on the other hand, there are experiments that have demonstrated that the end-tank stabilization technique is quite efficient. A detailed theory analysis is a matter of future work.

## VI. EFFECTS ASSOCIATED WITH THE ELECTRIC CONTACT OF THE PLASMA WITH THE END WALLS

The plasma present in the end tanks provides an electric contact between the main plasma and the conducting end surface. This contact may be good-enough to short circuit potential perturbations related to plasma motions (Eq. (14)) and thereby suppress the motion of the flux-tubes. The corresponding effect is commonly called “line-tying stabilization.” However, it has been understood long ago that the contact cannot be perfect due to the finite resistivity of the Debye sheath.<sup>61</sup> But even with that finite resistivity the stabilizing effect, as we shall see, can be significant, especially for the low- $m$  modes.

Another aspect of the electrical contact is that it allows controlling the unperturbed radial electric field by segmenting the end wall into a set of concentric rings electrically insulated from each other. They then can be biased independently thereby providing some degree of control over the plasma rotation; other effects are also possible (see below).

In this section, we consider an arbitrary distribution of the plasma parameters vs the radius (not necessarily step-wise as in Secs. V A–V C).

### A. Partial line-tying

We start from the discussion of high- $m$ , local modes and then make comments on the global  $m = 1$  mode. We consider the paraxial approximation as discussed in Sec. III B. Regarding the unperturbed state, we assume that there is no potential difference between the symmetric ends and, therefore, no unperturbed axial current. The unperturbed plasma has a potential  $\varphi_p$  with respect to the walls; this potential depends on the plasma parameters, with the strongest dependence on the electron temperature. As these parameters vary in the radial direction, so does the plasma potential, i.e., generally,  $\varphi_p = \varphi_p(r)$ . By  $\varphi_p$ , we mean the potential in the long (axisymmetric) confinement zone responsible for the instability.

When a plasma-filled flux tube moves to a new position, the plasma is advected with it and so does the plasma potential. The current to the end-plate appears only if the potential of the flux tube in a new position is different from the advected potential (we discuss the sources of this difference shortly). Therefore, in the linear problem, one obtains the following expression for the current to the end-wall:

$$\delta j_{\parallel} = \pm (\delta\varphi - \xi_{\perp} \cdot \nabla \varphi_p) \Sigma, \quad (58)$$

where  $\Sigma$  is a coefficient that characterizes the sheath electrical conductivity (it has a dimension of the conductivity

divided by length). We will dwell upon its structure and dependence on the plasma parameters later in this section. The sign convention is that the parallel current is positive if it flows towards the right end plate (in the positive  $z$  direction).

The last term in parenthesis is associated mainly with a gradient of the electron temperature, as the plasma potential is typically equal to a few  $T_e/e$ . Recalling Eq. (14), one finds that the ratio of the second term to the first term in Eq. (58) is of order  $m \frac{cT_e}{eBa_0^2\omega}$ . For the flute modes,  $|\omega| \sim \Gamma_0 \sim v_{Ti}/L$  (Eq. (29)). In other words, the ratio of the second to the first term is of order of  $(T_e/T_i)F_{FLR}$ , with  $F_{FLR}$  defined by Eq. (38). In a number of cases, the ratio  $T_e/T_i$  in the mirrors is significantly less than 1, meaning that

$$(T_e/T_i)F_{FLR} < 1, \quad (59)$$

so that the last term in Eq. (58) is small compared to the first term. Therefore, we start from the analysis of the situation where the second term can be neglected. It is this limit that describes a partial line-tying stabilization.

Using Eq. (25) and Eq. (58) with the last term neglected, one finds for the fastest growing modes

$$\frac{2i\omega \Sigma \delta\varphi}{c^2 B_W} = -\omega^2 I \frac{m^2 \delta\varphi}{\Psi} - m^2 D \delta\varphi, \quad (60)$$

where  $D$  and  $I$  are determined by Eq. (26), and we take into account that the currents to the end-plates have opposite signs at the right and the left ends. The resulting dispersion relation for the localized modes then becomes

$$\omega^2 + i\Gamma_1\omega + \Gamma_0^2 = 0, \quad (61)$$

where  $\Gamma_0$  is defined by Eq. (29) and  $\Gamma_1$  is

$$\Gamma_1 = \frac{2\Psi\Sigma}{m^2 c^2 B_W I}. \quad (62)$$

This is a positive quantity, signifying dissipative stabilization. If  $\Gamma_1$  is large compared to  $\Gamma_0$ , the growth rate becomes  $\text{Im}\omega \approx \Gamma_0^2/\Gamma_1$ , i.e., decreases by a factor

$$F_{LT} \equiv \frac{\Gamma_1}{\Gamma_0} \quad (63)$$

compared to non-conducting end-walls (the subscript “LT” stands for “line-tying”). In other words, although the instability still exists, its growth-rate may become small-enough to allow other stabilization techniques (e.g., feed-back, Sec. IX A); moreover, the slowly growing modes may be tolerable even without any additional stabilization if they lead to weak transport.

In order to separate the partial line-tying effect from the effects discussed in Sec. V A, we assume here that the stabilization by the favorable curvature in the end-tanks is absent (or insignificant); we neglect also the contribution of the end-tanks to the inertia.

To evaluate the figure of merit  $F_{LT}$ , we have to assess the processes that determine the parameter  $\Sigma$ . The current to the wall is controlled mostly by the Debye sheath at the wall, which repels the majority of the electrons, to make the total

unperturbed current zero. This means that, in the unperturbed state, the electron current is equal to the incoming ion current which is  $en_{wall}\sqrt{2W_i/m_i}$ , where  $n_{wall}$  is the plasma density near the wall (at the plasma side of the sheath). This current is not changed by the small variations of the wall potential. Conversely, the electron current is changed; for the Boltzmann electrons, the relative change of the electron current is  $e\delta\varphi/T_e$ . This leads to the following expression for  $\Sigma$  (Cf. Refs. 62 and 63):

$$\Sigma = C \frac{e^2 n_{wall}}{T_e} \sqrt{\frac{2W_i}{m_i}}. \quad (64)$$

We introduced an additional dimensionless coefficient  $C$  to account for possible deviations from the simple Boltzmann model for the electron response. Using Eq. (29) for  $\Gamma_0$ , evaluating  $I$  in Eq. (26) as  $m_i n L / 2B_0^2$  and relating  $n_{wall}$  to the density  $n$  in the confinement zone via the energy balance consideration (as it was done in conjunction with Eq. (53)), one finds

$$F_{LT} \approx \frac{4C}{m^2} \left( \frac{a}{\rho_i^{(e)}} \right)^2 \frac{L}{\tau_E \sqrt{2W_i/m_i}}. \quad (65)$$

Here,  $\rho_i^{(e)}$  is the ion gyro-radius evaluated for the electron temperature.

The electron distribution function in the end-tank has been analyzed in Refs. 20 and 21. It turns out that the average electron energy near the walls is a few times less than the electron temperature in the confinement zone, meaning that coefficient  $C$  in Eq. (64) is significantly greater than 1. We take a conservative value of  $C = 3$ . With that, the values of the parameter  $F_{LT}$  for the four fusion systems are presented in Table IV. From this table, one sees that the line-tying effects are significant for the first three systems, including the hybrid reactor. Note also that the high- $m$  modes are weakly affected by the partial line-tying. On the other hand, they are usually stabilized by the FLR effect (Sec. IV).

The results presented in Table IV are somewhat more optimistic than those of Ref. 60. The reason is the presence of a large coefficient  $C$  acting in the favorable direction and accounting for a relatively low electron temperature in the first three facilities. For the pure fusion system, the stabilizing effect is still insignificant.

Consider now the mode of a global displacement. For the displacement in the  $y$  direction considered in Sec. V, the last term in the brackets in Eq. (58) is proportional to  $y$ . Therefore, when substituted in the integrals in the l.h.s. of Eq. (47), it yields zero contribution. In this regard, in the case of a global mode, one does not need to impose a constraint (59) to neglect the last term in Eq. (58). We find then that dispersion relation (61) changes to

$$\omega^2 + i\Gamma_{1G}\omega + \Gamma_G^2 = 0. \quad (66)$$

A new dissipative term characterizing the line-tying for the global displacement mode  $\Gamma_{1G}$  is

$$\Gamma_{1G} = \frac{2\pi}{c^2 B_{wall}^5/2} \int \Psi \Sigma d\Psi, \quad (67)$$

where  $I_G$  is defined according to Eq. (49). If  $\Gamma_{1G}$  is large,  $\Gamma_{1G} \gg \Gamma_G$ , the growth rate is significantly reduced compared to  $\Gamma_G \sim \Gamma_0$ .

In the case of a global mode, the contribution of the large radii is much more pronounced than for  $m \gg 1$ . One can check (using Eq. (67)) that an additional large factor  $(a_{wall}/a_0)^3$  appears in the expression (65) for  $F_{LT}$  (with  $m = 1$ ). This factor makes  $F_{LT}$  much larger than one in all the cases of Table IV. However, this result has to be taken with caution, as we have here an interplay of two strong processes (two large parameters): the FLR effects that must be strong to force the  $m = 1$  mode to be a mode of the global displacement and the flux-tube flaring in the end tanks. We assumed here that the first one is decisively dominant. To obtain more reliable results one would have to solve a full equation for an eigenmode, with both FLR effects and strong flaring included. This has not been done yet.

One more factor that has to be looked at in this problem is the electron collisionality in the end tank. At high expansion ratio and high electron temperature (as in a fusion reactor), the electron-electron and electron-ion collision rates in the end tank become smaller than the expected growth rate of the instability. Then, variations of the current to the wall will include transitional processes, with a slow characteristic times, of order of collision times, and the model of an instantaneous reaction of the current through the sheath to the potential variation (Eq. (58)) becomes incorrect. An issue of the sheath current-voltage-characteristic under such circumstances has to be addressed. A factor that may restore a prompt reaction to the potential variation, is anomalous electron scattering produced by microfluctuations excited due to a non-Maxwellian character of the electron distribution in a weakly collisional plasma.<sup>20,21</sup>

There have not been recent experiments performed on the partial line tying. In the past, in a dedicated experiment,<sup>64</sup> the effect was favorable; it seemed to be in agreement with the general ideas of the role of partial line tying. Some line-tying stabilizing effect was also seen in a tandem mirror experiment.<sup>65</sup>

## B. The role of convective terms

In the previous discussion, we considered the situation where the electron temperature is sufficiently small, so that the last term in the r.h.s. of Eq. (58) can be neglected. This term describes a convective translation of the plasma potential: when the fluxtube with a plasma filling it is displaced

TABLE IV. The effect of the partial line-tying on the plasma stability.<sup>a</sup>

Device type	$(a/\rho_i^{(e)})^2$	$\sqrt{2W_i/m_i}$ $m/s$	$L/\tau_E \sqrt{2W_i/m_i}$	$(a_w/a)^3$	$F_{LT}$ Eq. (65)
GDT device	64	$1.7 \times 10^5$	$1.4 \times 10^{-2}$	$10^3$	$10/m^2$
Neutron source	$2.5 \times 10^3$	$3.3 \times 10^5$	$1.2 \times 10^{-3}$	$8 \times 10^3$	$36/m^2$
Hybrid driver	$2.1 \times 10^4$	$10^6$	$4 \times 10^{-5}$	$5 \times 10^2$	$10/m^2$
Pure fusion	$10^4$	$2 \times 10^6$	$4 \times 10^{-6}$	$10^3$	$0.5/m^2$

<sup>a</sup>The parameter  $C$  is taken to be 3. Other parameters are the same as in Tables I and III. The parameter  $(a_w/a)^3$  is presented to allow for evaluation of  $F_{LT}$  for the rigid displacement mode, as discussed after Eq. (67); the parameter  $F_{LT}$  characterizes the role of line-tying.

radially, its potential with respect to the end wall (which is determined by the plasma parameters inside the tube) is connected with it. Let us now address the case where this term is non-negligible. It turns out<sup>66,67</sup> that it leads to excitation of instabilities, which are not necessarily driven by the field-line curvature and are similar to dissipative drift instabilities. The strongest drive that acts even in the absence of curvature is the gradient of the electron temperature coupled with the sheath boundary condition. The instability is strongly affected by the change of the boundary conditions associated with the tilt of the end plates with respect to the field lines.<sup>68</sup> It may interfere both positively and negatively with short-wave-length curvature-driven perturbations and is not stabilized by FLR effects. This mode may be of significant importance in the tokamak scrape-off-layer. As this instability is of a quite a different nature than MHD instabilities, we will not go into the further detail. A review of it can be found in Ref. 69, together with further references.

We recall that for the mode of the global displacement, the integral of the last term over the surface of the end tank is identically zero due to the axial symmetry of the problem and the fact that for the uniform transverse displacement the term  $\xi_{\perp} \nabla \varphi_p$  in Eq. (58) disappears upon integration over  $dx dy$  for axisymmetric unperturbed state.

### C. Effect of electrostatic biasing

One can make the end plate in the form of concentric, mutually insulated rings and thereby acquire control over the radial potential distribution. In this case, one has to replace  $\varphi_p$  in Eq. (58) by  $\varphi_p + \varphi_b$ , where  $\varphi_b$  is a bias potential.

Electrostatic biasing allows one to control the plasma rotation, which can be characterized by a rotation frequency  $\Omega(\Psi)$ . In this section, we discuss a relatively slow rotation, where the centrifugal effects, which scale as  $\Omega^2$ , are still small (their role will be touched upon in Secs. VI D and VIII B).

Experiments with the GDT facility indicate that sufficiently strong positive biasing of the outer plasma surface leads to improved stability.<sup>70,71</sup> A theory developed by Beklemishev *et al.* relates this effect to a non-linear vortex stabilization,<sup>72,73</sup> where the shear flow developed in the region near the plasma boundary prevents the central part of the plasma from crossing this boundary. An alternative, more intuitive explanation, could be that the strong positive biasing of the outer layers creates a radial electrostatic potential barrier for the warm ion component; in the presence of the FLR effects (which make the plasma column “rigid”), this is enough to prevent the plasma from crossing this boundary. This whole issue deserves further studies along the lines of Refs. 66, 67 and 72.

In addition to the effects associated with the current flow to the end-walls, the biasing introduces also shear flow—a potentially stabilizing factor—in the bulk plasma. The dimensionless parameter that characterizes the effect of the shear flow is the ratio  $F_S$  of the shearing rate,  $r|d\Omega/dr|$  and the growth rate of the instability,  $\Gamma$ :  $F_S \equiv r|d\Omega/dr|/\Gamma_0$ . For the shearing effects to be significant, the first should be larger than the second,  $F_S \gg 1$ . In the situation where there is no forced biasing (the end-plates are grounded), one can expect

the potential difference between the axis and the outer boundary to be on the order of  $T_e/e$ . Then, the  $E \times B$  rotation velocity is of order of  $cT_e/aB$  and a shearing rate (provided there is of order one variation of the rotation frequency) is  $cT_e/a^2B$ . For the growth rate on the order of that determined by Eq. (29), one then obtains the following expression for  $F_S$ :

$$F_S = \frac{T_e(1+A)L\rho_i}{T_i a^2}, \quad (68)$$

where  $A = e[\varphi_b(r=0) - \varphi_b(r=a)]/T_e$ . Note that up to the  $T_e(I+A)/T_i$  factor, this is the same parameter that determines the role of FLR effects. In the situation where  $T_e=T_i$ , the shear-flow effects become important as soon as the FLR effects become important. In more general situations, where the electron and ion temperatures are unequal or the fast ions are present, this condition can somewhat shift one way or another. Depending on the sign of the imposed potential difference, the parameter  $A$  in Eq. (68) can be positive or negative. In the first case, the rotational velocity increases, whereas in the second case, it decreases and can be made zero; for strongly negative  $A$  the rotation reverses its direction.

Shear flow may drive its own, Kelvin-Helmholtz type of instabilities. In the situation described by Eq. (58), the interplay between the Kelvin-Helmholtz and other instabilities was studied in Ref. 74. Experiments performed on the Gamma 10 mirror device<sup>75</sup> seem to indicate that, at some level, the presence of the shear flow gives rise to reduced radial plasma losses.

### D. Fast rotation and centrifugal effects

When discussing plasma rotation in Sec. VI C, we assumed that the effect of rotation is related to the shear flow and concluded that this effect becomes significant under roughly the same conditions as the FLR effects. On the other hand, the rotation may have a more direct dynamical impact associated with the centripetal force. In an extreme case of a very rapid rotation, with rotation velocity exceeding the ion thermal velocity, it can even be used for what is called “centrifugal confinement:” the fast rotation would force the plasma to move to the equatorial plane of the mirror, where the plasma radius is maximum. Such a confinement technique has been studied most consistently in the experiments at Novosibirsk<sup>76</sup> and Maryland.<sup>77–79</sup> The shear in this rapid rotation may also provide improved flute stability.<sup>80–82</sup>

Stabilization can be also reached by a direct use of a centrifugal force.<sup>83</sup> The idea is that, if the plasma density has a depression near the axis, then the centrifugal force will have a stabilizing effect. The intuitively obvious stability condition is

$$m_i \Omega^2 r \frac{\partial n}{\partial r} > \kappa \frac{\partial p}{\partial r}. \quad (69)$$

For a long-thin mirror, with  $\kappa \sim a/L^2$ , the required density depression is quite small,  $\Delta n/n \sim (a/L)^2 (v_{Ti}/v_{rot})^2 \ll 1$ . It is assumed that at the plasma periphery, where the plasma pressure becomes small and the density would have to

decrease, a different stabilization technique can be used. As suggested in Ref. 80, this could, in particular, be achieved by creating a cold plasma annulus around the confinement zone; the annulus would be robustly stable by virtue of the line-tying to the ends. The practicality of this scheme has yet to be proven experimentally; indications of the favorable effect have been seen in Ref. 83.

In Ref. 84, a purely cylindrical problem with a radially decreasing density was considered so that the centripetal force was the only drive for the flute perturbations. It was found that the gradual shear has a generally stabilizing effect, whereas the abrupt jump in the angular frequency leads to excitation of Kelvin–Helmholtz modes.

The situation where plasma rotation is so fast that it may perturb the magnetic energy and drive the modes of “rotational ballooning” is considered in Sec. VIII B.

## VII. NON-PARAXIAL STABILIZERS

### A. Stability conditions

Stabilization techniques based on the presence of a significant amount of outflowing plasma can be effective in the relatively low- $Q$  mirror systems, like the neutron sources and, perhaps, hybrid fusion-fission systems. For high- $Q$  systems, the outflow is by necessity very small, and it is, therefore, interesting to assess stabilization techniques not relying on its presence. One such technique is based on sloshing ions (Sec. V B); however, for high- $Q$  fusion reactor parameters, it requires very high ion injection energy.

It turns out that favorable results can be attained by dropping the assumptions of the paraxiality of the system. There are two approaches of this type analyzed at some depth. One is based on the use of a divertor configuration built into a long-thin mirror; the other employs short-fat (i.e., non-paraxial) mirrors attached to a long-thin mirror. We will not consider more drastic departures from the paraxiality, like hollow, disk-like plasmas similar to those first considered by Furth<sup>85</sup> and Andreoletti<sup>86</sup> or switching to double-connected magnetic configurations (e.g., Ref. 87). A brief discussion of the earlier assessments of these more exotic geometries is presented in Ref. 2, where further references can be found. In other words, we focus on the “natural” linear geometry of mirrors.

We base our analysis on Eq. (17) with the last term in the r.h.s. dropped. From the MHD energy principle<sup>28</sup> and its drift-kinetic generalization<sup>88</sup> (ignoring for now FLR effects), one can show that the transition from stable to unstable plasma occurs at  $\omega=0$ . In other words, near the stability boundary, the plasma inside each flux tube has enough time to establish an equilibrium along the moving flux tube. In particular, in the important case of an isotropic plasma with  $p_{\parallel} = p_{\perp} = p$ , the pressure will be uniform along the field lines. The pressure perturbation will then consist of two terms: the convective term (which we already discussed, Eq. (24)) and the term determined by the adiabatic change of the flux-tube volume:

$$\delta p = -\xi_n Br [(\partial p / \partial \Psi) + \gamma p (\partial U / \partial \Psi) / U]. \quad (70)$$

The last term is expressly non-paraxial: it becomes negligible as soon as the change of the flux-tube volume in the course of its radial displacement becomes negligible. In the paraxial plasma with  $a \ll L$ , the length-scale of the radial pressure variation is  $a$ , whereas the length-scale of the radial variation of the specific volume is  $L$ , meaning that the last term is small.

Using Eq. (16) with no plasma outflow and Eqs. (17), (70), one obtains an eigen-equation that works near the stability boundary, i.e.,  $|\omega| \ll v_{Ti}/L$ :

$$-\frac{\partial}{\partial \Psi} I_1 \frac{\partial \varphi}{\partial \Psi} + m^2 \varphi I_2 + \frac{m^2 D}{\omega^2} \varphi = 0, \quad (71)$$

with

$$I_1 = \int \frac{r^2 \rho dl}{B}; \quad I_2 = \int \frac{\rho dl}{B^3 r^2}; \quad D = - \left[ \frac{\gamma p}{U} \left( \frac{dU}{d\Psi} \right)^2 + \frac{dp}{d\Psi} \frac{dU}{d\Psi} \right]. \quad (72)$$

The model of an almost isotropic pressure is good for high-mirror-ratio mirrors, without a large population of sloshing ions. One has, however, to remember that, in the course of displacement, the pressure remains isotropic (as we assumed) only if collisions are frequent; for motions at the time-scale shorter than collision time-scale the change of pressure in a flux tube of a complex shape does not necessarily have to be isotropic. This general case has been addressed, in particular, in Ref. 27.

Equation (71) yields a result analogous to Eq. (27)

$$\omega^2 = - \frac{m^2 \int D |\varphi|^2 d\Psi}{\int I_1 |\partial \varphi / \partial \Psi|^2 d\Psi + m^2 \int I_2 |\varphi|^2 d\Psi}. \quad (73)$$

Considering the localized, high  $m$  modes, one sees that the necessary and sufficient stability condition is

$$\frac{\gamma p}{U} \left( \frac{dU}{d\Psi} \right)^2 + \frac{dp}{d\Psi} \frac{dU}{d\Psi} > 0 \quad (74)$$

for all flux surfaces occupied by the plasma.<sup>89</sup> In the paraxial approximation, the second term is  $(L/a)^2$  times larger than the first term. Then, as  $U$  near the axis is a growing function of  $\Psi$ , we recover the unfavorable conclusion of Sec. III C. The first term, on the other hand, is universally stabilizing. Thus, for the configuration of a short-fat mirror, one can expect improved stability. The complete stabilization is, however, problematic. In magnetic confinement devices, we are interested in a plasma which is well separated from the walls. This means that the radial length-scale of the unperturbed pressure near the plasma boundary must be small compared to the plasma radius,  $|\delta p / \delta r| \gg p/a_0$ . In terms of the flux coordinate, this means that  $|\delta p / \delta \Psi| \gg p/\Psi_0$ . Consider, for example, an exponential pressure distribution near the boundary,  $p \propto \exp[-(\Psi - \Psi_0)/\Delta\Psi]$ , where  $\Psi_0$  characterizes the position of the boundary, with  $\Delta\Psi \ll \Psi_0$  characterizing the width of the transition zone. Substituting this distribution to Eq. (74), one finds that the first term contains

a small factor  $\Delta\Psi/\Psi_0$  compared to the second, and the boundary is still unstable. In other words, the switch to a short-fat mirror does not lead by itself to stabilization.

Two factors may lead to a more favorable conclusion. First, one can consider a non-paraxial mirror attached at two ends of a long paraxial linear system producing strong FLR effects, as described in Ref. 27. Then, the only mode that remains potentially unstable is the mode of a global displacement, and the stability condition becomes less stringent than Eq. (74) (see Sec. VII B). Second, if the specific volume  $U(\Phi)$  has a singularity as a function of  $\Phi$  near the plasma boundary, the ordering of the terms in Eq. (74) may change. This can be reached, in particular, by the creation of a cusp magnetic field near the boundary which would look like a tokamak divertor configuration. These possibilities are considered in Secs. VII C and VII D.

## B. Short-fat mirror attached to the solenoid

The general shape of the magnetic geometry is illustrated in Fig. 8. The specific structure of the magnetic surfaces in the end cells may be different from that shown in Fig. 8, which is just one of the possible examples.

Before formulating the stability criterion, we make rough estimates of the relative contributions of the central cell and the anchor cells to the coefficient  $D$ , Eq. (72). These cells will be separated by strong mirrors, so that the plasma pressures in them ( $p_0$  and  $p_a$ ) can be different from each other, with the pressures being almost isotropic. Here and below the subscript “a” refers to the anchor cell. The length and the radius of the anchor cells are  $L_a$  and  $a_a$ , respectively, with  $a_a \leq L_a$ ; the equality sign is reached in the case of a non-paraxial cell which we will eventually be most interested in. By noting that

$$\left(\frac{\partial U}{\partial \Psi}\right)_0 \sim \frac{L_0 a_0^2}{\Psi B_0 L_0^2}, \quad \left(\frac{\partial U}{\partial \Psi}\right)_a \sim \frac{L_a a_a^2}{\Psi B_a L_a^2} \quad (75)$$

for the central section and the anchor sections, respectively, and using the flux conservation  $a_a^2 B_a \sim a_0^2 B_0 \sim \Psi$ , one can evaluate the contributions to  $D$  from the central cell and the anchor cells

$$D_0 \sim \frac{p_0}{\Psi L_0 B_0^2}, \quad D_a \sim \frac{p_a}{\Psi L_a B_a^2}. \quad (76)$$

For a non-paraxial anchor, one has to take  $L_a \sim a_a$ . Regarding the inertia, we assume that it is determined by a long central section

$$I_2 \sim \frac{\rho_0 L_0}{\Psi B_0^2}. \quad (77)$$

As was mentioned in Sec. VII A, the non-paraxial mirror does not stabilize localized modes, but, if properly designed, may stabilize the global mode. This is achieved if  $D_a$  exceeds  $D_0$  by the absolute value,  $|D_a| = q|D_0|$ , with  $q > 1$ . The parameter  $q$  plays a role of a “safety margin” for the global mode. By comparing expressions for  $D_0$  and  $D_a$ , Eq. (76), one sees that

$$q \sim \frac{\beta_a L_0}{\beta_0 L_a}. \quad (78)$$

The MHD growth rate for higher  $m$  modes would be

$$\Gamma \sim \sqrt{\frac{|D_a|}{I_2}} \sim \sqrt{q} \frac{v_{Ti}}{L_0}. \quad (79)$$

According to Eq. (37), in order for them to be stabilized by FLR effects in the central cell, the condition

$$(m/2)F_{FLR} > \sqrt{q} \quad (80)$$

has to be satisfied. This condition is more stringent than condition  $(m/2)F_{FLR} > 1$ . For the example of a fusion reactor presented in Table I, for  $m=2$  mode,  $(m/2)F_{FLR}$  is  $\sim 2$  (see Table II), so that  $q$  is limited to the values below  $\sim 4$ .

If condition (80) holds with some margin, the only mode that may remain unstable is the mode of a rigid displacement in the long solenoid. In other words, the potential perturbation has the form  $\varphi = \chi\sqrt{\Phi}$ , with  $\chi$  being some constant. In this case, the numerator in Eq. (73) becomes

$$\begin{aligned} \int D|\varphi|^2 d\Psi &= -|\chi|^2 \int \left[ \frac{\gamma p}{U} \left( \frac{dU}{d\Psi} \right)^2 + \frac{dp}{d\Psi} \frac{dU}{d\Psi} \right] \Psi d\Psi \\ &= -|\chi|^2 \int \left[ \frac{\gamma \Psi}{U} \left( \frac{dU}{d\Psi} \right)^2 - \frac{d}{d\Psi} \left( \Psi \frac{dU}{d\Psi} \right) \right] p d\Psi. \end{aligned} \quad (81)$$

It is sufficient to have the square bracket in the last integral positive at some  $\Psi$ : then, the pressure peaked near these values of  $\Psi$  will make the whole system stable with respect to the global mode. Near the axis, the square bracket is universally negative, as it becomes  $-U' < 0$  at  $\Psi \rightarrow 0$ . Therefore, indeed, only non-paraxial effects can lead to the stabilization.

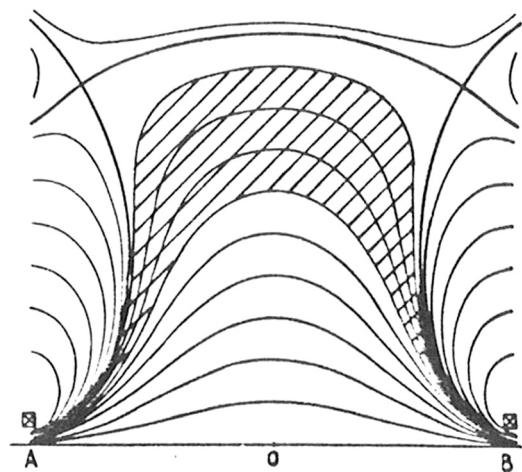


FIG. 8. A “short-fat” mirror as a stabilizer of a global mode. The plasma boundary has to be situated well within the separatrix passing through the null points. This ensures the conservation of the adiabatic invariant over the whole confinement region. The area where the boundary can be situated is shaded. If the boundary is closer to the axis than the shaded area, the non-paraxiality effects become weak and the system becomes unstable. A long confinement cell is attached to the stabilizer through one of the mirrors. The second stabilizer is situated at the opposite end of the confinement zone.

Specific examples of non-paraxial magnetic field possessing the stabilizing property were presented in Ref. 27. It was also shown that non-isotropic particle distributions in the non-paraxial mirrors can lead to stabilization. However, due to the lack of resources, no designs of particular coil systems were developed and no experimental tests have been made.

On the other hand, this whole approach begs for more detailed analyses, as the anchors possess “natural” geometry and can be combined with ambipolar plugs in tandem mirrors. Also, this stabilization technique is based on the well-established physics.

**C. Cusp stabilizers**

The magnetic configuration in question is shown in Fig. 9. Here, unlike Sec. VII B, it is assumed that the plasma extends to the singular flux surface, where the magnetic null is situated. This geometry is similar to the poloidal field geometry near the divertor nulls in tokamaks and is sometimes referred to as a “divertor stabilizer.” We start from a purely MHD analysis based on Eq. (74).

According to Eq. (74), the marginal stability pressure profile (corresponding to  $D = 0$ ) is

$$p = \text{const}/U^\gamma. \tag{82}$$

As  $U$  diverges at  $r \rightarrow r_0$  (Fig. 9), one could expect that this critical profile would correspond to a rapidly enough decrease of the plasma pressure near the boundary surface. One can see that when approaching the singular flux surface, the function  $U$  varies as

$$U = \alpha_1 L_0/B_0 + \alpha_2 (a_0/B_0) \ln \frac{r_0}{r_0 - r}, \tag{83}$$

where  $\alpha_1$  and  $\alpha_2$  are positive constants of order one and  $r$  and  $r_0$  are the radius of a flux surface and the radius of the critical flux surface (separatrix), both at large distances from the divertor along the axis (Fig. 9). Representation (83) “works” in the vicinity of the separatrix, at small  $r_0 - r$ . The pressure profile (82) is illustrated in Fig. 10 by a black line. A more general analysis, accounting for the particle anisotropy, was made in Ref. 90.

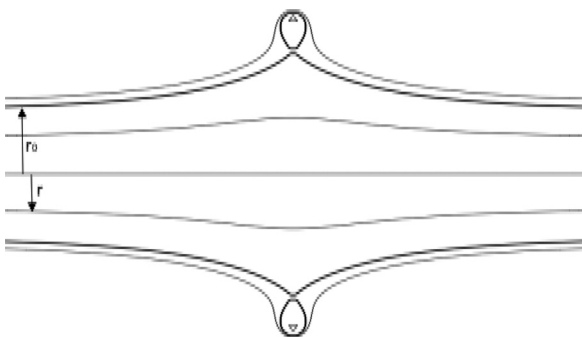


FIG. 9. A cusp stabilizer. This particular configuration is obtained by superposing a uniform solenoidal field and the field of a single coil with the current in a direction opposite to the current in the solenoid (solenoid is not shown). The solenoid continues to the left and to the right where it is ended by strong mirrors. The distance of a flux surface from the axis in the region of a uniform field is  $r$ , the distance of the separatrix is  $r_0$ .

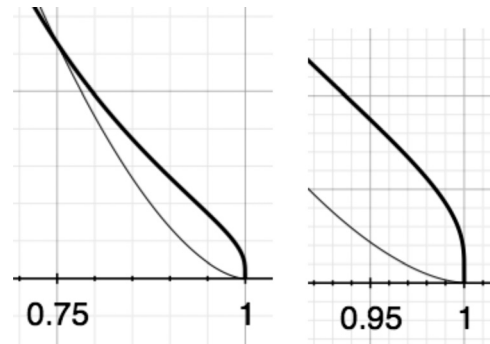


FIG. 10. Normalized critical pressure profiles (82) for the simple divertor of Fig. 9 (bold line) and the snowflake divertor of Fig. 11 (thin line), A.U. The profiles correspond to the same pressure at  $r = r_0/2$ . The abscissa axis is  $r/r_0$ . The right panel shows vicinity of the separatrix.

A potential problem associated with this technique is the presence of the magnetic field null that gives rise to violation of the adiabatic invariant near the separatrix; the axial particle life-time in this zone becomes much shorter than the confinement time in the plasma core. This means that the plasma pressure at the separatrix will be much smaller than the pressure in the confinement zone. For a linear dependence of pressure vs  $r_0 - r$ , as is the case of diffusive losses, with the pressure vanishing at the separatrix, the second (destabilizing) term in Eq. (74) diverges faster than the first term, meaning the re-appearance of the flute instability near the separatrix. Alternatively, one has to assume that some small plasma pressure is present even at and beyond the separatrix, with the confinement time determined by rapid axial losses, like in the tokamak scrape-off layer.

Of some interest in this regard can be creating a second-order magnetic field null, where not only the field but also its first spatial derivatives would become zero (Fig. 11). In tokamaks such a divertor is called a “snowflake divertor,”<sup>91</sup> due to a hexagonal symmetry of the magnetic field near the null. In such a case, an analog of Eq. (83) is

$$U = \alpha_1 L_0/B_0 + \alpha_2 (r_0/B_0) \left( \frac{r_0}{r_0 - r} \right)^{1/3}. \tag{84}$$

A stronger divergence of  $U$  gives rise to a somewhat smoother critical pressure profile (Fig. 10, thin line), so that the plasma pressure at the separatrix required for the stabilization of linear pressure profile becomes smaller.

Interestingly, the critical pressure profile (82) may be satisfactory for the plasma confinement in a levitated dipole.<sup>92</sup> In this case,  $U$  scales as  $r^{-4}$ , where  $r$  is the distance of the flux surface from the center. The inner plasma boundary is stable because the pressure here drops in the direction of decreasing  $U$ . The critical pressure profile on the external side is  $p \propto r^{-4\gamma} \propto r^{-20/3}$ . Note that there is no singularity at large distances. The pressure may reach negligible values at not-too-large values of  $r$ , making this configuration quite interesting for the magnetic confinement. Experiments with such a plasma are reported in Refs. 92 and 93.

Returning to the cusp stabilizers in linear mirror devices, one can try to exploit effects that go beyond the MHD

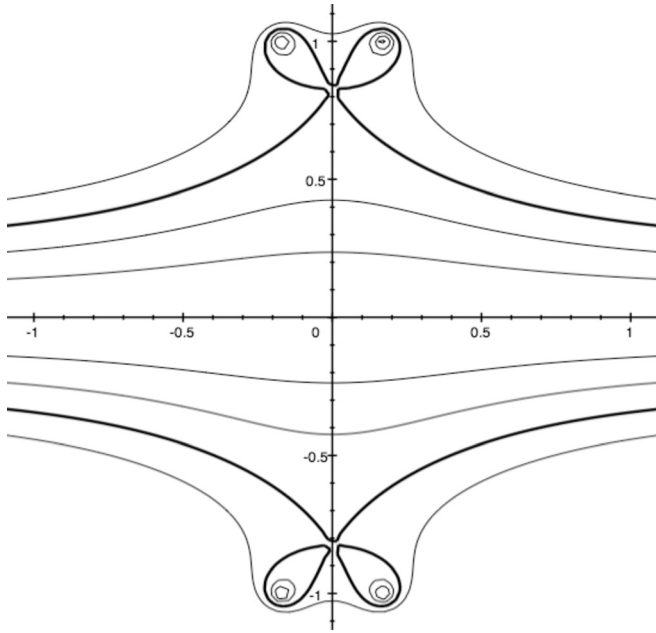


FIG. 11. A snowflake divertor. Both the magnetic field and its first derivatives are zero in the singular point. To get such configuration, one has to split the coil of Fig. 9 into two coils and properly adjust the distance between them.

description. In particular, in Ref. 94, rapid azimuthal electron drift near the null-point was supposed to short-circuit the  $m=1$  perturbations, whereas the higher mode numbers would be suppressed by the FLR effects. This concept has been recently analyzed<sup>95</sup> as an option for the Gamma-10 mirror facility. Detailed description of the corresponding magnetic system and possible plasma equilibria was presented in Ref. 96, and the structure of MHD fluctuations for unstable equilibria was studied numerically in Ref. 97. This geometry will be used in a divertor-simulator version of a rebuilt GAMMA-10 facility.<sup>98</sup>

Experimentally, Casey *et al.*<sup>99</sup> have observed partial stabilization of the plasma with magnetic divertor on the TARA facility. Significant reduction of the  $m=1$  mode amplitude has been obtained on the HIEI facility.<sup>100</sup> More recently, a modest favorable effect was found in the experiments with the HANBIT facility.<sup>101</sup>

In general, the divertor approach seems interesting and promising, although the creation of divertors in the mirror reactor environment may be not a trivial task, because of the effect on the adiabaticity of fast ions and problems with plasma loss through the vicinity of the null-point. Note that the aforementioned experiments were performed with a plasma with a temperature in the range of a few tens of electron-volts and low plasma densities.

#### D. Multi-cusp systems

One can stabilize the axisymmetric mirror by applying a multi-cusp magnetic field near the plasma surface, by a set of neighboring coils each creating a configuration similar to that of Fig. 9. This would allow creating a linear confinement zone, which could be plugged at the ends by two choke coils.

This approach has been assessed in 1960s–1970s in combination with electrostatic plugging of multiple slits that appear in this cusp configuration.<sup>102</sup> For review of this approach see Ref. 103.

In this case, a magnetic field would have favorable curvature over the entire plasma boundary. The practicality of electrostatic confinement for fusion reactor conditions may, however, be an issue.

In an elegant LAMEX experiment,<sup>104</sup> Fig. 12, there was no electrostatic plugging of the plasma leaking through the vicinity of the null-points. The plasma had  $T_e \sim 5$  eV,  $5 \text{ eV} < T_i < 60 \text{ eV}$ ,  $5 \times 10^9 \text{ cm}^{-3} < n < 5 \times 10^{11} \text{ cm}^{-3}$ , so that possible plasma leaks through the nulls were not of a concern. The plasma confinement obeyed the classical axial loss through a strong mirror and no gross MHD instability was present. Extrapolation of this technique to fusion reactor conditions may be non-trivial.

The LAMEX experiment allowed obtaining experimental data on the scaling of the mirror confinement vs the mirror ratio, up to the mirror ratios of  $R=74$ , in various collisionality regimes.<sup>105</sup> A linear scaling was found at high mirror ratios for collisional-enough plasmas, in agreement with the theory of gas-dynamic confinement.<sup>14</sup>

### VIII. FINITE-BETA EFFECTS

#### A. Wall stabilization of the finite-beta plasma

At small values of the parameter  $\beta$ , the plasma motions are accompanied by only small perturbations of the magnetic field, which are of order of  $\beta$ . When one couples these magnetic field perturbations with the plasma currents, which are also of the order of  $\beta$ , one finds that the corrections to the force acting on the plasma are of order of  $\beta^2$ , whereas the pressure forces that we have considered thus far are of order  $\beta$ . In other words, magnetic field perturbations in a sufficiently low beta plasma are small and will not produce stability unless there are other small parameters in the stability problem, with which the effects of a small (albeit finite beta) can compete.

A natural parameter could be the paraxiality, Eq. (18). To beat the instability in a paraxial system, it is tempting to put a conducting wall around the plasma and rely on the image currents that would be produced by the plasma

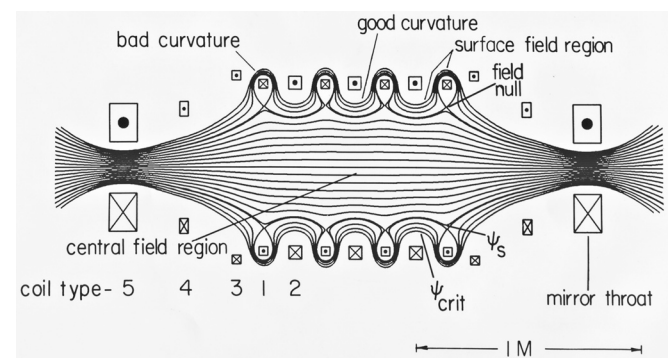


FIG. 12. Magnetic field lines and coils of the Large Axisymmetric Mirror Experiment (LAMEX). The field lines shown are for the configuration  $B_z = 200$  G and mirror ratio 20. Courtesy J.R. Ferron, Ref. 104.

displacements and would provide restoring (stabilizing) force. However, this force itself will contain a small paraxiality parameter. Indeed, if one considers a purely cylindrical geometry, without the  $z$  variations, the plasma lateral displacement does not produce magnetic field perturbations outside the plasma (Fig. 13). However, as a purely cylindrical geometry is marginally stable, the deviation from a cylinder, within the paraxial approximation needs to be considered. It of course leads to the flute destabilization effect that is first order in the paraxial parameter  $a^2 a/d\ell^2$  and in beta. Conducting wall stabilization terms also come in to first order in the paraxial parameter, but, as noted, second order in beta.

So, using the finite-beta effects for the stabilization is by far not a trivial matter. A possible solution to these problems was described in Ref. 106 where an analysis was made of a hot plasma whose axial velocity spread is more narrowly confined than the magnetic field. Ref. 106 assumed that the radius of a conducting shell surrounding the plasma is not-too-large, so that the gap between the hot plasma and the wall is comparable or smaller than the plasma radius. Then, the global lateral displacement of the plasma will induce image currents in the wall and generate the restoring force roughly leading to the finite  $\beta$  stabilization condition  $\beta \geq (L_H/L)^2$ , where  $L_H$  is the hot plasma axial scale length and  $L$  is the axial scale length of the vacuum magnetic mirror field (note that in the paraxial stability scaling the axial scale length,  $L_H$ , needs to be larger than the plasma radius). This stabilizing factor may be sufficient for the stabilization of the whole device above a critical beta value, although an auxiliary mechanism is still required to get the system above the threshold beta value. Detailed calculations can be found in Ref. 106, and the theory was extended to arbitrary beta in Ref. 110.

Robust finite-beta stabilization can be produced by using a short-fat stabilizer with a closely fitting conducting shell.<sup>107</sup> There will be a gap between the shell and the wall but the gap will be small compared to the plasma radius. Then, a global plasma displacement does produce the magnetic field perturbation in the gap; and a strong restoring force appears, especially as beta approaches unity, where the restoring force is proportional to  $(1 - \beta_\perp)^{-2}$ . This mecha-

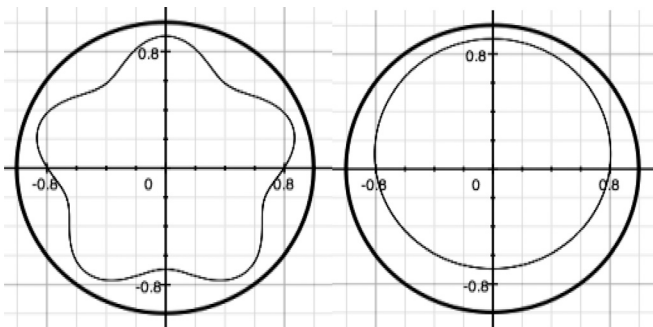


FIG. 13. The cross-section of a cylindrical conducting shell and a plasma with  $m = 5$  and  $m = 1$  perturbations. The magnetic field is directed along the axis of the cylinder. In a purely cylindrical case, for linear perturbations, the magnetic field outside the plasma is not perturbed (remains uniform and parallel to the axis), and no restoring force appears.

nism works most efficiently for the global displacement modes, as the high- $m$  modes create perturbations that rapidly decay away from the plasma surface, and, at order unity beta, are driven by the larger equilibrium curvature rather than the smaller vacuum field curvature.<sup>106</sup> The higher- $m$  modes would, however, be stabilized by the FLR effects in the presence of a long-thin central mirror cell. The conducting wall can occupy only part of the whole length of the non-paraxial system and still produce a noticeable stabilizing effect.<sup>108</sup>

The use of a finite-beta stabilization would require the use of some other stabilization techniques during the start-up phase, as getting a finite beta plasma during the time short compared to the low-beta instability growth would need very high heating power in fusion-grade devices.

## B. Ballooning effects

In Sec. VIII A, we considered stabilizing effects associated with the finite plasma pressure. The flip side of the finite- $\beta$  effects is that they can drive MHD instabilities in the regimes stable at small  $\beta$ . This is of a concern for the systems with long-thin central cells stabilized at the ends by some type of anchors. Consider, for example, the situation shown in Fig. 14, where the central cell is line-tied at the left end, whereas the other end is free. In a small- $\beta$  flute approximation, this system would be stable. But a finite- $\beta$  plasma may possess sufficient free energy to bend gently the plasma column causing only a minor perturbation of the magnetic energy and allowing for the thermal energy release in the zone of the unfavorable curvature at the right end. This energy release would be the same as for a pure flute displacement. As the perturbation is related to the bending of a thin plasma column reminiscent of bending of a bicycle tire, this mode is often called a “ballooning mode.”

The magnetic energy perturbation for the deformation shown in Fig. 14 is associated with the tilting of the magnetic field lines and can be evaluated as

$$\delta W_{\text{magn}} \sim \pi a^2 L \left( \frac{\xi}{L} \right)^2 \frac{B^2}{8\pi}, \quad (85)$$

where  $\xi$  is the displacement of the right end. On the other hand, the release of the plasma energy at the unstable end is

$$\delta W_{\text{Therm}} \sim \pi a^2 L_1 \left( \frac{\xi}{L_1} \right)^2 p, \quad (86)$$

where  $L_1$  (Fig. 14) is the length of the transition region between the solenoid and the mirror. By comparing Eqs. (85) and (86), one finds that a system with a large distance

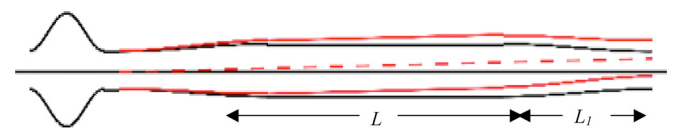


FIG. 14. (Color online) Ballooning perturbation in the system stabilized at one end only. At zero beta the system is stable but it becomes unstable if beta exceeds the limit determined by Eq. (87).

between the stabilizing element and unstable section is unstable if

$$\beta > \frac{L_1}{L}, \quad (87)$$

which can be significantly less than 1. The recipe should be to have another anchor near the unstable section.

Indeed, for the axisymmetric cell anchored at both ends, the quantitative assessment presented in Refs. 12 and 109 leads to critical values of beta close to 1. At this point, the axisymmetric mirrors again demonstrate their advantage over the systems with quadrupole anchors: in the latter case, due to the presence of strong fanning regions (see Fig. 2), there appears an additional small parameter in the magnetic energy perturbation for the bends in the direction of a small thickness,<sup>12,13,110</sup> leading to critical  $\beta$  values significantly less than 1.

Plasma ballooning can also lead to the release of the plasma rotation energy. A rotational ballooning mode can develop in the systems with a long solenoidal section, like a reactor version of GDT.<sup>14</sup> In long solenoids, the higher- $m$  modes can be stabilized by FLR effects, but the  $m = 1$  mode is still of concern. The rotational instability of this mode must involve the bending of the plasma column (whence a term “rotational ballooning”): a pure translation, obviously, just moves plasma from one equilibrium to another, identical to the first, just shifted. Indeed, as an insightful analysis presented in Refs. 111 and 112 shows the mode with an axial mode number  $n = 1$  is most prominent. The instability criterion can be roughly formulated as

$$\rho v_{rot}^2 > \frac{B^2}{8\pi} \left(\frac{a}{L}\right)^2. \quad (88)$$

Detailed numerical simulations of this mode are presented in Ref. 35. If the system contains a long solenoid, condition (87) may become quite restrictive; a cure could be a rotation control by segmenting the end plates, as discussed in Sec. V.

### C. Fire-hose and mirror instabilities

At higher values of beta, approaching unity, two fast instabilities may show up: a firehose instability<sup>113</sup> and a mirror instability.<sup>114</sup> The first one is present when the parallel pressure significantly exceeds the perpendicular pressure. The stability criterion with respect to this mode reads as

$$p_{||} - p_{\perp} < \frac{B^2}{4\pi}. \quad (89)$$

This instability is important for the design of the neutron source based on a strongly tilted ion injection, at a shallow angle with respect to the magnetic axis.

The mirror instability is related to the fact that high-beta plasma produces a depression of the magnetic field strength due to the plasma pressure. If the distribution function has a significant anisotropy, as may be the case of sloshing ions near their turning points, the local field depression leads to a further piling up of the ions in the region of the weakened magnetic field. The stability criterion is

$$B \frac{dp_{\perp}}{dB} < \frac{B^2}{4\pi}. \quad (90)$$

Mirror instability severely limits the MHD stabilization by sloshing ions. It is also folded into design constraints of mirror neutron sources. An insightful discussion of the bifurcated equilibria appearing when condition (90) is broken is presented on Ref. 115.

## IX. OTHER STABILIZATION TECHNIQUES

### A. Feedback stabilization

It is a challenge to use feedback control to stabilize flute modes in mirror devices. First, the instability is very fast. For a tandem mirror reactor plug, the growth rate would be in the range  $10^6 \text{ s}^{-1}$ . Second, localized flute perturbations do not cause significant perturbations of magnetic or electric field outside the plasma, so it is hard to detect these modes to provide an input for the feedback system. Third, for basically the same reason, it is hard to engage the fusion plasma by a feedback actuator, especially if one deals with high- $m$  modes. Thus it seems that in order to use the feedback technique, the flute perturbations have first to be at least partially stabilized by one of the techniques mentioned earlier. Then, if only the global perturbation remains active and has a reduced growth-rate, the feedback stabilization may become feasible.

In the presence of electrical contact of the plasma with end plates, one could use segmented end plates to affect the plasma potential inside the confinement zone. The finer the segmentation, the higher modes can be affected. To the authors' knowledge, this approach has not yet been assessed for a fusion reactor environment.

In the 1960s and 1970s, a feedback stabilization has been tried with some success on several mirror devices (see a review Ref. 116), at a relatively low plasma density. After that, a broad use of quadrupole stabilizers has led to virtual abandonment of the feedback stabilization in mirror research. Very recently, a small-scale experiment has been built in Israel<sup>117</sup> to study a stabilization of a global flute mode with the use of optical sensors and electro-magnetic actuators. Related theoretical efforts are underway.<sup>118</sup>

### B. Ponderomotive stabilization

The ponderomotive stabilization is based on the use of an external force acting on the plasma. To have a stabilizing effect, the perturbation of this force has to be of a restoring nature. Consider, as an example, a simple axisymmetric mirror, without contact to the end walls and therefore unstable by itself. Let it be subject to the action of an additional force. It has to be axisymmetric in the unperturbed state, but its reaction to plasma perturbations (in particular, density perturbations), does not have to be axisymmetric. It will lead to an appearance of the additional term  $\delta f_{add\perp}^{(p)}$  in Eq. (17); here the superscript “p” corresponds to “ponderomotive.” Let us assume that this term has a simple form:

$$\delta f_{add\perp}^{(p)} = -\alpha_1 \xi_{\perp} - \alpha_2 \dot{\xi}_{\perp}. \quad (91)$$

The signs are chosen in such a way that the positive  $\alpha$ 's correspond to a restoring force. Expression (91) can have a

more complex structure, in particular, can contain a term proportional to  $\hat{z} \times \xi_{\perp}$ , but we limit our discussion by a simpler equation (91). The coefficients  $\alpha_{1,2}$  depend on the plasma parameters and become zero outside the plasma.

The most obvious target for the ponderomotive stabilization is the global mode; the higher- $m$  modes could be left to the mercy of FLR effects. For the global mode, repeating the steps described in Sec. III, we find instead of Eq. (48):

$$\omega^2 + i\nu^{(p)}\omega + \Gamma_G^2 - \Gamma_G^{(p)2} = 0, \quad (92)$$

with

$$\nu^{(p)} = I_G^{-1} \int \frac{dz}{B^{7/2}} \alpha_2 d\Phi, \quad \Gamma_G^{(p)2} = I_G^{-1} \int \frac{dz}{B^{7/2}} \alpha_1 d\Phi. \quad (93)$$

The global mode is stabilized if  $\alpha_1$  is large enough; the presence of the term  $\alpha_2$  does not lead to stabilization but may significantly reduce the growth rate if  $\alpha_2 \gg \Gamma_G$ .

A favorable effect of a ponderomotive force produced by RF oscillations was detected on several facilities, including Phaedrus<sup>119</sup> and HIEI.<sup>120</sup> On the first of them, the stabilizing effect was present at the frequencies both above<sup>121</sup> and below<sup>122</sup> the ion cyclotron frequency. Theory and simulations of the radio-frequency stabilization were discussed in Refs. 123–125. In Ref. 126, it was suggested to use for the stabilization a force imparted to the plasma by neutral beams injected in the approximately radial direction. The effect was found noticeable in the case of long devices.

When assessing possible use of the ponderomotive stabilization in a specific fusion device, one has to analyze the effect of this technique on both the velocity-space instabilities and particle scattering and on drift-type instabilities responsible for the plasma cross-field transport. Note that application of the known transport scalings to mirrors yields generally favorable results.<sup>127,128</sup>

## X. DISCUSSION AND SUMMARY

There are many techniques that can make an axisymmetric mirror device MHD stable or at least significantly reduce the growth rate. Some of them have been tested experimentally, the other exist only as general concepts supported by more or less detailed theory analyses. The existence of this broad range of approaches is important and beneficial for mirror fusion, because different devices may be best suited for different stabilization techniques. One has to remember that, in any fusion device, in addition to the gross MHD stability, which is a backbone of success, there are many other constraints required for its good performance. Among them are (i) a tolerable level of cross-field transport driven by drift-type instabilities and (ii) the absence of fast velocity-space instabilities, like the loss-cone instabilities. When the latter two issues are taken care of, it may turn out that some of the MHD stabilization methods cannot be applied. For example, if too narrow pitch-angle particle distribution is needed, it may become incompatible with velocity-space microstability.

Also important are constraints imposed by the operational scenarios: it may be difficult to maintain a fine balance

between the plasma parameters in different parts of the device (as required by some stabilization techniques) during the start-up phase, although it may become possible to maintain this balance in the steady state operation. One more type of constraints stems from the difficulty of creating the magnets and vacuum vessels for confining plasmas of too complex shapes. Therefore, it is indeed helpful to have a broad variety of the MHD-stabilization techniques as described in our paper.

All in all, the most desirable stabilization techniques are those that are compatible with a natural, cigar-like shape of the confinement zone, possibly with additional shorter cells attached at the ends. With that, preferable are stabilization techniques relying on passive stabilization and using the naturally existing geometries and distribution functions.

Mirror facilities with a small fusion gain  $Q$ , like neutron sources and divertor simulators, can be stabilized by the experimentally proven techniques based on the use of the outflowing plasma. Facilities with modest  $Q$ , like fusion drivers for fusion-fission hybrids or actinide burners, may benefit from the stabilization via line-tying, although additional stabilization techniques would be needed to suppress the residual instability. Pure-fusion systems with high  $Q$  require the use of the built-in stabilizers, like non-paraxial mirror cells or divertor stabilizers. The efficiency of these techniques has yet to be demonstrated in the facilities with fusion-relevant plasma parameters.

The test of stabilization techniques suitable for high- $Q$  systems can be performed based on axisymmetric facilities of the type of the GDT device at Novosibirsk. Adding new stabilizing elements to the system where one can control the plasma outflow is the most straightforward way for checking the workability of the stabilizer: one can gradually pinch the outflow off and thereby reduce or even eliminate the stabilizing contribution of the plasma in the end tank. It is here where the advantage of the axial symmetry shows up: adding an axisymmetric element to an already axisymmetric system can be done without making any significant changes to the rest of the facility. So, the GDT and other axisymmetric devices routinely operating with fusion-relevant plasmas<sup>129</sup> can serve as a platform for definitive tests of some of the concepts mentioned in our paper.

It is important to emphasize that the process of designing, building, and testing axisymmetric mirror devices is greatly accelerated by their intrinsic engineering simplicity, as mentioned in Introduction. Reaching a definitive conclusion on whether the mirrors can or cannot become a viable fusion reactor would require not many decades but less than 10 years.<sup>18</sup> This is why the axisymmetric mirrors keep attracting the interest of researchers, even though the current scale of the theory and experimental work on mirrors, worldwide, is quite modest.

## ACKNOWLEDGMENT

This article is based on a tutorial presented at 2010 APS DPP Annual Meeting. The authors are grateful to C. Bolton for support of this work and to N. Hershkowitz, J. Kesner, M. Koepke, and M. Mauel for helpful suggestions. This work was performed under the auspices of the U.S.

Department of Energy by Lawrence Livermore National Laboratory under Contract DE-AC52-07NA27344.

## APPENDIX A: SOME USEFUL GEOMETRICAL RELATIONS

We assume that the magnetic field is curl-free,  $\nabla \times \mathbf{B} = 0$ . One then has

$$(\mathbf{B} \cdot \nabla)\mathbf{B} = \frac{1}{2}\nabla B^2. \quad (\text{A1})$$

On the other hand,

$$(\mathbf{B} \cdot \nabla)\mathbf{B} = B(\mathbf{t} \cdot \nabla)\mathbf{t} = \mathbf{B} \left( \mathbf{t} \frac{\partial \mathbf{B}}{\partial \ell} + n \frac{\partial \mathbf{B}}{\partial n} \right). \quad (\text{A2})$$

Together with Eq. (1), this leads to Eq. (6). Other useful relations are

$$\nabla \cdot \left( \frac{\mathbf{n}}{r} \right) = -\frac{\partial B(\Psi, s)}{\partial \Psi}; \quad (\text{A3})$$

$$\nabla \cdot \mathbf{t} = \nabla \cdot \left( \frac{\mathbf{B}}{B} \right) = -\frac{1}{B} \frac{\partial B}{\partial \ell}; \quad (\text{A4})$$

and

$$\frac{d}{d\Psi} \int_{-\infty}^{\infty} g(\Psi, \ell) d\ell = \int_{-\infty}^{\infty} \frac{1}{r} \frac{\partial}{\partial n} \left[ \frac{g}{B} \right] d\ell, \quad (\text{A5})$$

where  $g$  as a function of  $\ell$  vanishes rapidly enough beyond the confinement zone.

We note that the pressure force is

$$\begin{aligned} f_x = & -\frac{\partial p_{x\beta}}{\partial x_\beta} = -\delta_{x\beta} \frac{\partial p_\perp}{\partial x_\beta} + t_x t_\beta \frac{\partial p_\perp}{\partial x_\beta} \\ & + p_\perp \left( t_x \frac{\partial t_\beta}{\partial x_\beta} + t_\beta \frac{\partial t_x}{\partial x_\beta} \right) - t_x t_\beta \frac{\partial p_\parallel}{\partial x_\beta} - p_\parallel \left( t_x \frac{\partial t_\beta}{\partial x_\beta} + t_\beta \frac{\partial t_x}{\partial x_\beta} \right). \end{aligned} \quad (\text{A6})$$

The parallel projection of the force in the equilibrium is zero,  $t_x f_x = 0$ . Noting that  $t_x \partial t_x / \partial x_\beta = 0$  and using Eqs. (A4) and (A6), one then finds Eq. (4). Written in vectorial notation (e.g.,  $\delta_{x\beta} \partial p_\perp / \partial x_\beta \rightarrow \nabla p_\perp$ ), Eq. (A6) yields Eq. (10).

The normal projection of the pressure force is

$$\mathbf{n} \cdot \mathbf{f} = -\mathbf{n} \cdot \nabla p - \kappa(p_\parallel - p_\perp), \quad (\text{A7})$$

where we accounted for Eq. (A2) and the identity  $n_x t_x = 0$ .

We now derive Eq. (17). We substitute Eq. (14) in the first term of Eq. (15); taking divergence, we obtain the first term in Eq. (17). The divergence of the second term in Eq. (15) yields

$$\begin{aligned} c \nabla \cdot \left[ \frac{\mathbf{B}}{B^2} \times \nabla \delta p_\perp \right] &= c \left[ \nabla \times \frac{\mathbf{B}}{B^2} \right] \cdot \nabla \delta p_\perp \\ &= \frac{2c}{B^3} [\mathbf{B} \times \nabla B] \cdot \nabla \delta p_\perp, \end{aligned} \quad (\text{A8})$$

where we have taken into account that  $\nabla \times \mathbf{B} = 0$ . One can note also that the vector  $[\mathbf{B} \times \nabla B]$  has only  $\vartheta$  component (along the bi-normal  $\mathbf{b}$ ),  $[\mathbf{B} \times \nabla B] = \mathbf{b} B \partial B / \partial n$ , so that

$[\mathbf{B} \times \nabla B] \cdot \nabla \delta p_\perp = (B/r)(\partial B / \partial n)(\partial \delta p_\perp / \partial \vartheta)$ . Similarly, in the third term in Eq. (15),  $[\mathbf{B} \times (\mathbf{t} \cdot \nabla)\mathbf{t}] = \mathbf{b} \kappa B = \mathbf{b} \partial B / \partial n$  (here we used Eq. (6)). As the divergence of  $\mathbf{b}$  is zero, the divergence of the third term in Eq. (15) yields

$$\begin{aligned} (c/B)(\partial B / \partial n)[\mathbf{b} \cdot \nabla(\delta p_\parallel - \delta p_\perp)] \\ = (c/Br)(\partial B / \partial n) \partial(\delta p_\parallel - \delta p_\perp) / \partial \vartheta. \end{aligned} \quad (\text{A9})$$

Combining these results, one obtains the second term in the r.h.s. of Eq. (17).

## APPENDIX B: A COMPUTATIONAL TOOL FOR DETERMINING AXISYMMETRIC MIRROR EQUILIBRIUM AND STABILITY IN THE PARAXIAL LIMIT—THE FLORA CODE

A magnetohydrodynamic equilibrium and stability code for paraxial, axisymmetric mirror configurations including finite  $\beta$ , finite-Larmor-radius, and rotation effects, FLORA, was developed at Lawrence Livermore National Laboratory in the 1980s based on Newcomb's paraxial theory of stability for the frequencies below the ion gyrofrequency.<sup>31–34</sup> Newcomb's theory was elaborated by Cohen, Freis, and Newcomb for axisymmetric tandem mirrors in Ref. 35, and the FLORA code was introduced. Equations for the equilibrium, Euler-Lagrange equations for nonlinear and linear stability, and the FLORA code embodying the equilibrium and linear stability equations are presented in Ref. 33. FLORA continues to be used, e.g., in the more recent computations of the kinetic stabilizer concept for axisymmetric mirrors,<sup>131</sup> and we give a brief overview of FLORA here.

The paraxial theory of equilibrium and stability of an axisymmetric mirror system on which the FLORA code is based is given in Ref. 35. The lowest-order perpendicular pressure balance condition (30) is used to compute the self-consistent magnetic field  $B(\Psi, z)$  in terms of the perpendicular pressure  $p_\perp(\Psi, z)$  and the axial vacuum magnetic field  $B_{\text{vac}}(z)$ . The pressure (summed over species) can be deduced from a model velocity distribution function, Eq. (3), and the axial vacuum field can be deduced from a model of the current coils.

The perpendicular and parallel pressure are related by the parallel pressure balance condition (4). We note that  $B^2 = B_z^2 + O(\varepsilon^2)$ , where  $\varepsilon$  is defined by Eq. (18). In order that the equilibrium is well posed, stability to the firehose and mirror modes must be imposed, Eqs. (89) and (90).

An ambipolar potential profile  $\varphi(\Psi, z)$  must be provided which can be determined by imposing quasineutrality or a simple model electric potential can be used. In practice,  $p_\parallel(B, \Psi)$ ,  $B_{\text{vac}}(\Psi, z)$ , and  $\varphi(\Psi, z)$  are input to the equilibrium computations. FLORA has simple model profiles for  $p_\parallel(B, \Psi)$ ,  $B_{\text{vac}}(z)$ , and  $\varphi(\Psi, z)$  with coefficients that are controlled by input parameters. FLORA has provisions for two or three-region tandem mirror configurations, composed of center cell, choke cell, and end plug cell regions, controlled by the specification of the input profiles.

FLORA solves the linearized Euler–Lagrange equations for the incompressible displacement of the plasma, Eq. (41) in Ref. 35 in the time domain for a single azimuthal Fourier mode with mode number  $m$  in the  $(\Psi, z)$  domain using centered, second-order-accurate finite differencing for the

spatial derivatives in stretched coordinates  $u(z)$  and  $v(\Psi)$  to facilitate better spatial resolution where needed. The stability equation solved accommodates finite Larmor radius; finite plasma pressure (finite beta); rotational effects due to  $\mathbf{E} \times \mathbf{B}$ , diamagnetic drift, and  $\nabla B$  drift; and magnetic curvature. The low-beta, high- $m$  limit of Eq. (41) in Ref. 35 recovers an eigenequation having the same structure as Eq. (37). The stability equation in FLORA is a partial differential equation with second-order time derivatives for real and imaginary parts of the plasma displacement (assumed to be incompressible). The terms associated with the shear-Alfvén wave are solved implicitly to relax the Courant-Friedrichs-Lewy condition that would otherwise limit the time step. The real and imaginary parts of the stability equation are solved iteratively for the real and imaginary parts of the plasma displacement. The iteration is convergent if the time step resolves the real part of the mode frequency. The stability equation is solved as an initial-value problem: after initialization the most-unstable mode naturally emerges after a few e-foldings unless the forms of the initial perturbations are pathological. We note that solving the initial-value problem in the time domain to determine the stability/instability boundary becomes impractical as one approaches the marginal stability boundary in parameter space (an e-folding time approaches infinity as marginal stability is approached). To determine marginal stability with FLORA, one must use extrapolation of the observed growth rates to zero as a function of the parameters, which implies multiple simulations.

The properties of the paraxial stability equation are illustrated in several analytical and numerical examples in Ref. 35. Analytical results are presented in the low-beta limit for high  $m$ , for a two-region plasma with square profiles in  $\Psi$  wall effects and for a class of special profiles leading to a solution in terms of Bessel functions. Numerical results were obtained with FLORA for the stability of a rotating  $\theta$ -pinch (as in Refs. 108); a model tandem mirror equilibrium; stability with hot electrons (low-density, rigid electrons with finite-beta well digging, and no charge uncovering effects); and stability with a cold, line-tied halo plasma.<sup>33</sup> Additional numerical examples of FLORA were published in Refs. 45 and 130. Caponi *et al.* addressed the stabilizing effects of finite Larmor radius combined with contact with a lateral wall or with a line-tied cold-plasma blanket using parameters relevant to a symmetric tandem mirror experiment.<sup>45</sup> Dobrott *et al.* examined the stability of an axisymmetric tandem mirror with energetic electron rings or disks (low-density, rigid electrons), finite Larmor radius, and a lateral wall included. Byers resurrected and extended FLORA to study the kinetic stabilizer concept.<sup>131</sup> FLORA can be obtained from Cohen at Lawrence Livermore National Laboratory, and there is a user's manual available.<sup>132</sup>

<sup>1</sup>R. F. Post, *Nucl. Fusion* **27**, 1579 (1987).

<sup>2</sup>D. D. Ryutov, *Sov. Phys. Uspekhi* **31**, 300 (1988).

<sup>3</sup>N. Hershkovitz, S. Miyoshi, and D. D. Ryutov, *Nucl. Fusion* **30**, 1761 (1990).

<sup>4</sup>R. F. Post and D. D. Ryutov, *Comments Plasma Phys. Controlled Fusion* **16**, 375 (1995).

<sup>5</sup>Yu. V. Gott, M. S. Ioffe, and V. G. Telkovsky, *Nuclear Fusion (Suppl. 3)*, 1045 (1962).

<sup>6</sup>B. G. Logan, J. F. Clauser, F. H. Coensgen, D. L. Correll, W. F. Cummins, C. Gormezano, A. W. Molvik, W. E. Nexsen, T. C. Simonen, B. W. Stallard, and W. C. Turner, *Phys. Rev. Lett.* **37**, 1468 (1976).

<sup>7</sup>T. C. Simonen, J. F. Clauser, F. H. Coensgen, D. L. Correll, W. F. Cummins, J. H. Foote, A. H. Futch, R. K. Goodman, D. P. Grubb, A. L. Hunt, A. W. Molvik, W. E. Nexsen, B. W. Stallard, W. C. Turner, R. P. Drake, and G. Melin, paper presented at the Seventh International Conference on Plasma Physics and Controlled Nuclear Fusion Research, Innsbruck, Austria, September 1978 (IAEA, Vienna); *Nucl. Fusion* **2**, 389 (1979).

<sup>8</sup>T. C. Simonen, *Proc. IEEE* **69**, 935 (1981).

<sup>9</sup>G. I. Dimov, V. V. Zakaidakov, and M. E. Kishinevskii, *Sov. J. Plasma Phys.* **2**, 597 (1976); G. I. Dimov, *Phys. Usp.*, **48**, 1129 (2005).

<sup>10</sup>T. K. Fowler and B. G. Logan, *Comments Plasma Phys. Controlled Fusion* **2**, 167 (1977).

<sup>11</sup>D. D. Ryutov and G. V. Stupakov, *JETP Lett.* **26**, 3, 174 (1977); *Sov. Phys. Dokl.* **23**, 412 (1978); R. H. Cohen, *Nucl. Fusion* **19**, 1579 (1979).

<sup>12</sup>D. D. Ryutov and G. V. Stupakov, paper presented at the Eighth International Conference on Plasma Physics and Controlled Nuclear Fusion Research, Brussels, Belgium, 1980 (IAEA, Vienna, 1981), Vol. 1, p. 119.

<sup>13</sup>T. B. Kaiser and L. D. Pearlstein, *Phys. Fluids* **26**, 3053 (1983).

<sup>14</sup>V. V. Mirnov and D. D. Ryutov, *Sov. Tech. Phys Lett.* **5**, 279 (1979).

<sup>15</sup>A. A. Ivanov, A. D. Beklemishev, E. P. Kruglyakov, P. A. Bagryansky, A. A. Lizunov, V. V. Maximov, S. V. Murakhtin, and V. V. Prikhodko, *Fus. Sci. Technol.* **57**, 320 (2010).

<sup>16</sup>D. D. Ryutov, *Plasma Phys. Controlled Fusion* **32**, 999 (1990).

<sup>17</sup>A. Molvik, A. Ivanov, G. I. Kulcinski, D. Ryutov, J. Santarius, T. Simonen, B. D. Wirth, and A. Ying, *Fusion Sci. Technol.* **57**, 369 (2010).

<sup>18</sup>T. C. Simonen, *Fusion Sci. Technol.* **57**, 305 (2010).

<sup>19</sup>D. E. Baldwin, *Rev. Mod. Phys.* **49**, 317 (1977).

<sup>20</sup>D. D. Ryutov, *Fusion Sci. Technol.* **47**, 148 (2005).

<sup>21</sup>D. D. Ryutov, A. W. Molvik, and T. C. Simonen, *J. Fusion Energy* **29** (2010).

<sup>22</sup>P. A. Bagryansky, A. V. Anikeev, and A. D. Beklemishev, *Fusion Sci. Technol.* **59**, 31 (2011).

<sup>23</sup>G. F. Bogdanov, I. N. Golovin, Y. A. Kucheryaev, and D. A. Panov, *Nucl. Fusion, (Suppl. 1)*, 215 (1962).

<sup>24</sup>V. D. Shafranov, *Reviews of Plasma Physics*, edited by M. A. Leontovich (Consultants Bureau, New York, 1966), Vol. 2, p. 103.

<sup>25</sup>J. D. Jackson, *Classical Electrodynamics* (John Wiley & Sons, New York, 1975).

<sup>26</sup>M. N. Rosenbluth and C. L. Longmire, *Ann. Phys.* **1**, 120 (1957).

<sup>27</sup>D. D. Ryutov and G. V. Stupakov, *JETP Lett.* **42**, 35 (1985); *Sov. J. Plasma Phys.* **12**, 815 (1986).

<sup>28</sup>I. B. Bernstein, E. A. Frieman, M. D. Kruskal, and R. M. Kulsrud, *Proc. R. Soc. London, Ser. A* **244**, 17 (1958).

<sup>29</sup>L. D. Landau and E. M. Lifshitz, *Fluid Mechanics* (Pergamon Press, Oxford, 1987).

<sup>30</sup>V. P. Nagornyy, D. D. Ryutov, and G. V. Stupakov, *Nucl. Fusion* **24**, 1421 (1984).

<sup>31</sup>W. A. Newcomb, *Nucl. Fusion (Suppl. 2)*, 451 (1962).

<sup>32</sup>W. A. Newcomb, *Ann. Phys. (N.Y.)* **81**, 231 (1973).

<sup>33</sup>W. A. Newcomb, *J. Plasma Phys.* **26**, 529 (1981).

<sup>34</sup>W. A. Newcomb, *Phys. Fluids* **28**, 505 (1985).

<sup>35</sup>B. I. Cohen, R. P. Freis, and W. A. Newcomb, *Phys. Fluids* **29**, 1558 (1986).

<sup>36</sup>F. L. Hinton and M. N. Rosenbluth, *Nucl. Fusion* **22**, 1547 (1982).

<sup>37</sup>R. F. Post, *Trans. Fusion Sci. Technol.* **35**, 40 (1999).

<sup>38</sup>R. F. Post, *Trans. Fusion Sci. Technol.* **43**, 195 (2003).

<sup>39</sup>R. F. Post, *Fusion Sci. Technol.* **51**, 112 (2007).

<sup>40</sup>R. F. Post, *Fusion Sci. Technol.* **57**, 335 (2010).

<sup>41</sup>M. N. Rosenbluth, N. A. Krall, and N. Rostoker, *Nucl. Fusion (Suppl. 1)*, 143 (1962).

<sup>42</sup>K. V. Roberts and J. B. Taylor, *Phys. Rev. Lett.* **8**, 197 (1962).

<sup>43</sup>L. I. Rudakov, *Nucl. Fusion* **2**, 107 (1962).

<sup>44</sup>S. I. Braginski, *Reviews of Plasma Physics*, edited by M. A. Leontovich (Consultants Bureau, New York, 1965).

<sup>45</sup>M. Z. Caponi, B. I. Cohen, and R. P. Freis, *Phys. Fluids* **30**, 1410 (1987).

<sup>46</sup>A. A. Ivanov, A. V. Anikeev, P. A. Bagryansky, V. N. Bocharov, P. P. Deichuli, A. N. Karpushov, V. V. Maximov, A. A. Podminogin, A. I. Rogozin, T. V. Salikova, and Yu. A. Tsidulko, *Phys. Plasmas* **1**, 1529 (1994).

<sup>47</sup>A. V. Anikeev, P. A. Bagryansky, P. P. Deichuli, A. A. Ivanov, A. N. Karpushov, V. V. Maximov, A. A. Podminogin, N. V. Stupishin, and Y. A. Tsidulko, *Phys. Plasmas* **4**, 347 (1997).

<sup>48</sup>T. C. Simonen, S. L. Allen, T. A. Casper, J. F. Clauser, C. A. Clower, F. H. Coensgen, D. L. Correll, W. F. Cummins, C. C. Damm, M. Flammer, J. H. Foote, R. K. Goodman, D. P. Grubb, E. B. Hooper, R. S. Hornady, A. L. Hunt, R. G. Kerr, A. W. Molvik, R. H. Munger, W. E. Nexsen, T. J.

- Orzechowski, W. L. Pickles, P. Poulsen, M. E. Rensink, B. W. Stallard, W. C. Turner, W. L. Hsu, W. Bauer, T. L. Yu, and D. Zimmermann, *Phys. Rev. Lett.* **50**, 1668 (1983).
- <sup>49</sup>T. C. Simonen, *Nucl. Fusion* **25**, 1205 (1985).
- <sup>50</sup>B. I. Cohen, N. Maron, and W. M. Nevins, *Phys. Fluids* **27**, 642 (1984).
- <sup>51</sup>B. I. Cohen, G. R. Smith, N. Maron, and W. M. Nevins, *Phys. Fluids* **26**, 1851 (1983).
- <sup>52</sup>I. A. Kotelnikov, G. V. Roslyakov, and D. D. Ryutov, *Sov. J. Plasma Phys.* **13**, 227 (1987).
- <sup>53</sup>B. B. Kadomtsev and O. P. Pogutse, *Sov. Phys. Dokl.* **14**, 470 (1969).
- <sup>54</sup>H. L. Berk, M. N. Rosenbluth, H. V. Wong, T. M. Antonsen, and D. E. Baldwin, in *Proceedings of the Ninth International Conference on Plasma Physics and Controlled Nuclear Fusion Research, Baltimore, MD* (IAEA, Vienna, 1983), Vol. 2, p. 175; H. L. Berk, M. N. Rosenbluth, H. V. Wong, and D. E. Baldwin, *Sov. J. Plasma Phys.* **9**, 108, (1983).
- <sup>55</sup>J. Kesner, R. S. Post, B. D. McVey, and D. K. Smith, *Nucl. Fusion* **22**, 549 (1982).
- <sup>56</sup>H. L. Berk and J. Pratt, *Nucl. Fusion* **51**, 083025 (2011).
- <sup>57</sup>H. L. Berk, M. N. Rosenbluth, R. H. Cohen, and W. M. Nevins, *Phys. Fluids* **28**, 2824 (1985).
- <sup>58</sup>R. H. Cohen, W. M. Nevins, and H. L. Berk, *Phys. Fluids* **29**, 1578 (1986).
- <sup>59</sup>H. L. Berk and G. V. Stupakov, *Phys. Fluids B* **3**, 440 (1991).
- <sup>60</sup>R. Scarmozzino, A. K. Sen, and G. A. Navratil, *Phys. Rev. Lett.* **57**, 1729 (1986).
- <sup>61</sup>W. B. Kunkel and J. U. Guillery, in *Proceeding of the Seventh Conference on the Phenomena in Ionized Gases, Belgrade, 1965*, edited by B. Perovic and D. Tosic (Gradevinska Knjiga, Belgrade, Yugoslavia, 1966), Vol. II, p. 702.
- <sup>62</sup>T. B. Kaiser and B. I. Cohen, *Phys. Fluids* **30**, 1564 (1987).
- <sup>63</sup>D. D. Ryutov, in *Proceedings of the Course and Workshop, Varenna, Italy* (Editrici Compositori, Bologna, 1987), Vol. II, p. 791.
- <sup>64</sup>A. W. Molvik, R. A. Breun, S. N. Golovato, N. Hershkovitz, B. McVey, R. S. Post, D. Smatlak, and L. Yujiri, *Phys. Fluids* **27**, 2711 (1984).
- <sup>65</sup>A. W. Molvik, J. D. Barter, D. A. Buchenauer, T. A. Casper, D. L. Correll, G. Dimonte, S. Falabella, H. Foote, and P. A. Pincosy, *Nucl. Fusion* **30**, 815 (1990).
- <sup>66</sup>H. L. Berk, D. D. Ryutov, and Yu. A. Tsidulko, *JETP Lett.* **52**, 23 (1990).
- <sup>67</sup>H. L. Berk, D. D. Ryutov, and Yu. A. Tsidulko, *Phys. Fluids B* **3**, 1346 (1991).
- <sup>68</sup>D. Farina, R. Pozzoli, and D. D. Ryutov, *Plasma Phys. Controlled Fusion* **35**, 1271 (1993).
- <sup>69</sup>R. H. Cohen, B. LaBombard, D. D. Ryutov, J. L. Terry, M. V. Umansky, X. Q. Xu, and S. Zweben, *Nucl. Fusion* **47**, 612 (2007).
- <sup>70</sup>P. A. Bagryansky, A. A. Lizunov, A. A. Zuev, E. Yu. Kolesnikov, and A. L. Solomachin, *Fusion Sci. Technol.* **43**, 152 (2003).
- <sup>71</sup>P. A. Bagryansky, A. D. Beklemishev, and E. I. Soldatkina, *Fusion Sci. Technol.* **51**, 340 (2007).
- <sup>72</sup>A. D. Beklemishev, Joint Varenna-Lausanne International Workshop on Theory of Fusion Plasmas, Aug. 25–29, 2008, Varenna, Italy; *AIP Conf. Proc.* **1069**, 3 (2008).
- <sup>73</sup>A. D. Beklemishev, P. A. Bagryansky, M. S. Chaschin, and E. I. Soldatkina, *Fusion Sci. Technol.* **57**, 351 (2010).
- <sup>74</sup>K. Lotov, D. Ryutov, and J. Weiland, *Phys. Scr.* **50**, 153 (1994).
- <sup>75</sup>T. Cho, M. Yoshida, J. Kohagura *et al.*, *Phys. Rev. Lett.* **94**, 085002 (2005).
- <sup>76</sup>A. A. Bekhtenev, V. I. Volosov, V. E. Pal'chikov, M. S. Pekker, and Y. N. Yudin, *Nucl. Fusion* **20**, 579 (1980).
- <sup>77</sup>J. Ghosh, R. C. Elton, H. R. Griem, A. Case, A. W. DeSilva, R. F. Ellis, A. Hassam, R. Lunsford, and C. Teodorescu, *Phys. Plasmas* **13**, 022503 (2006).
- <sup>78</sup>C. Teodorescu, W. C. Young, G. W. S. Swan, R. F. Ellis, A. B. Hassam, and C. A. Romero-Talamas, *Phys. Rev. Lett.* **105**, 085003 (2010).
- <sup>79</sup>S. Choi, P. N. Guzdar, A. Case, R. Ellis, A. B. Hassam, R. Lunsford, C. Teodorescu, and I. Uzun-Kaymak, *Phys. Plasmas* **15**, 042507 (2008).
- <sup>80</sup>B. N. Breizman and F. A. Tsel'nik, *Sov. Plasma Phys.* **9**, 666 (1983).
- <sup>81</sup>Y.-M. Huang and A. B. Hassam, *Phys. Plasmas* **11**, 2459 (2004).
- <sup>82</sup>S. W. Ng and A. B. Hassam, *Phys. Plasmas* **12**, 064504 (2005).
- <sup>83</sup>V. N. Bocharov, N. A. Zavadskii, A. V. Kiselev, S. G. Konstantinov, A. M. Kudryavtsev, O. K. Myskin, V. M. Panasyuk, and F. A. Tsel'nik, *JETP Lett.* **41**, 601 (1985).
- <sup>84</sup>T. D. Rognien, *J. Appl. Phys.* **44**, 3505 (1973).
- <sup>85</sup>H. P. Furth, *Phys. Rev. Lett.* **11**, 308 (1963).
- <sup>86</sup>J. Andreoletti, *Comptes Rendus* **257**, 1235 (1963).
- <sup>87</sup>V. V. Arsenin, *Trans. Fusion Technol.* **35**, 3 (1999).
- <sup>88</sup>M. D. Kruskal and C. R. Oberman, *Phys. Fluids* **1**, 275 (1958).
- <sup>89</sup>B. B. Kadomtsev and C. R. Oberman, *Reviews of Plasma Physics*, edited by M. A. Leontovich, (Consultants Bureau, NY, 1965), Vol. 2, p. 153.
- <sup>90</sup>V. V. Arsenin and A. Y. Kuyanov, *Plasma Phys. Rep.* **27**, 635 (2001).
- <sup>91</sup>D. D. Ryutov, *Phys. Plasmas* **14**, 064502 (2007).
- <sup>92</sup>J. Kesner, M. S. Davis, J. L. Ellsworth, D. T. Garnier, J. Kahn, M. E. Mauel, P. Michael, B. Wilson, and P. P. Woskov, *Plasma Phys. Controlled Fusion* **52**, 124036 (2010).
- <sup>93</sup>D. T. Garnier, A. C. Boxer, J. L. Ellsworth *et al.*, *Nucl. Fusion* **49**, 055023 (2009).
- <sup>94</sup>B. Lane, R. S. Post, and J. Kesner, *Nucl. Fusion* **27**, 277 (1987).
- <sup>95</sup>V. P. Pastukhov, *Fusion Sci. Technol.* **47**, 138 (2005).
- <sup>96</sup>I. Katanuma, Y. Sasagawa, Y. Tatematsu, Y. Nakashima, T. Cho, and V. P. Pastukhov, *Nucl. Fusion* **46**, 608 (2006).
- <sup>97</sup>I. Katanuma, K. Yagi, Y. Nakashima, M. Ichimura, and T. Imai, *Phys. Plasmas* **17**, 032303 (2010).
- <sup>98</sup>Y. Nakashima, H. Takeda, R. Yonenaga, K. Hosoi, H. Ozawa, T. Ishii, N. Nishino, M. Ichimura, T. Kariya, I. Katanuma, R. Minami, Y. Miyata, Y. Yamaguchi, M. Yoshikawa, and T. Imai, *Fusion Sci. Technol.* **59**, 61 (2011).
- <sup>99</sup>J. A. Casey, B. G. Lane, J. H. Irby, K. L. Brau, S. N. Golovato, W. C. Guss, J. Kesner, R. S. Post, E. Sevillano, and J. Zielinski, *Phys. Fluids* **31**, 2009 (1988).
- <sup>100</sup>Y. Yasaka, A. Maruyama, and N. Takano, *Fusion Sci. Technol.* **43**, 44 (2003).
- <sup>101</sup>A. C. England, D. K. Lee, S. G. Lee, M. Kwon, S. W. Yoon, Y. Yasaka, N. Sugimoto, I. Katanuma, K. Yashiro, and T. Imai, *Nucl. Fusion* **49**, 125008 (2009).
- <sup>102</sup>O. A. Lavrentiev, *Ukr. Fiz. Zhurnal* **18**, 1019 (1973).
- <sup>103</sup>T. J. Dolan, *Plasma Phys. Controlled Fusion* **36**, 1539 (1994).
- <sup>104</sup>J. R. Ferron, A. Y. Wong, G. Dimonte, and B. J. Leikind, *Phys. Fluids* **26**, 2227 (1983).
- <sup>105</sup>K. L. Lam, B. J. Leikind, A. Y. Wong, G. Dimonte, A. Kuthi, L. Olson, and H. Zwi, *Phys. Fluids* **29**, 3433 (1986).
- <sup>106</sup>H. L. Berk, M. N. Rosenbluth, H. V. Wong, T. M. Antonsen, Jr., *Phys. Fluids* **27**, 2705 (1984).
- <sup>107</sup>J. Kesner, *Nucl. Fusion* **25**, 275 (1985).
- <sup>108</sup>X. Z. Li, J. Kesner, and B. Lane, *Nucl. Fusion* **27**, 101 (1987).
- <sup>109</sup>T. B. Kaiser and L. D. Pearlstein, *Phys. Fluids* **28**, 1003 (1985).
- <sup>110</sup>T. B. Kaiser, W. M. Nevins, and L. D. Pearlstein, *Phys. Fluids* **26**, 351 (1983).
- <sup>111</sup>J. P. Freidberg and L. D. Pearlstein, *Phys. Fluids* **21**, 1207 (1978).
- <sup>112</sup>L. D. Pearlstein and J. P. Freidberg, *Phys. Fluids* **21**, 1218 (1978).
- <sup>113</sup>E. N. Parker, *Phys. Rev.* **109**, 1874 (1958).
- <sup>114</sup>W. B. Thompson, *An Introduction to Plasma Physics* (Pergamon, NY, 1964), p. 216.
- <sup>115</sup>I. A. Kotelnikov, *Trans. Fusion Sci. Technol.* **59**, 47 (2011).
- <sup>116</sup>V. V. Arsenin and V. A. Chuyanov, *Uspekhi* **123**, 83 (1977).
- <sup>117</sup>A. Lifshitz, I. Be'ery, A. Fisher, and A. Ron, *Bull. Am. Phys. Soc.* **55**, 56 (2010).
- <sup>118</sup>I. Be'ery, A. Lifshitz, A. Fisher, and A. Ron, *Bull. Am. Phys. Soc.* **55**, 56 (2010).
- <sup>119</sup>J. R. Ferron, N. Hershkovitz, B. A. Breun, B. N. Golovato, and R. Goulding, *Phys. Rev. Lett.* **51**, 1955 (1983).
- <sup>120</sup>Y. Yasaka and R. Itatani, *Phys. Rev. Lett.* **56**, 2811 (1986).
- <sup>121</sup>S. Meassick, T. Intrator, N. Hershkovitz, J. Browning, and R. Majeski, *Phys. Fluids B* **1**, 1049 (1989).
- <sup>122</sup>J. I. Browning, N. Hershkovitz, T. Intrator, R. Majeski, and S. Meassick, *Phys. Fluids B* **1**, 1692 (1989).
- <sup>123</sup>J. R. Myra and D. A. D'Ippolito, *Phys. Rev. Lett.* **53**, 914 (1984).
- <sup>124</sup>P. L. Similon and A. N. Kaufman, *Phys. Rev. Lett.* **53**, 1061 (1984).
- <sup>125</sup>N. F. Otani and B. I. Cohen, *Phys. Fluids* **31**, 158 (1988).
- <sup>126</sup>I. A. Kotelnikov, A. Masliev, D. D. Ryutov, and S. Shaikhislamov, *Sov. J. Plasma Phys.* **16**, 669 (1990).
- <sup>127</sup>J. Pratt and W. Horton, *Phys. Plasmas* **13**, 042513 (2006).
- <sup>128</sup>J. Pratt, W. Horton, and H. L. Berk, *J. Fusion Energy* **27**, 91 (2008).
- <sup>129</sup>A. V. Burdakov, A. A. Ivanov, and E. P. Kruglyakov, *Plasma Phys. Controlled Fusion* **52**, 124026 (2010).
- <sup>130</sup>D. Dobrott, S. Kendrick, R. P. Freis, and B. I. Cohen, *Phys. Fluids* **30**, 2149 (1987).
- <sup>131</sup>R. F. Post, T. K. Fowler, R. Bulmer, J. Byers, D. Hua, and L. Tung, *Fusion Sci. Technol.* **47**, 49 (2005).
- <sup>132</sup>R. P. Freis and B. I. Cohen, "User's Manual for the FLORA Equilibrium and Stability Code," Lawrence Livermore National Laboratory (UCID-20400), April 1, 1985.